ADVANCED REVIEW

WIREs COMPUTATIONAL MOLECULAR SCIENCE WILEY

Modeling of the spectroscopy of core electrons with density functional theory

Nicholas A. Besley 🟢

School of Chemistry, University of Nottingham, University Park, Nottingham, UK

Correspondence
Nicholas A. Besley, School of Chemistry, University of Nottingham, University Park, Nottingham, NG7 2RD, UK.
Email: nick.besley@nottingham.ac.uk

Funding information
N/A

Edited by: Anna Krylov, Associate Editor

Abstract

The availability of X-ray light sources with increased resolution and intensity has provided a foundation for increasingly sophisticated experimental studies exploiting the spectroscopy of core electrons to probe fundamental chemical, physical, and biological processes. Quantum chemical calculations can play a critical role in the analysis of these experimental measurements. The relatively low computational cost of density functional theory (DFT) and time-dependent density functional theory (TDDFT) make them attractive choices for simulating the spectroscopy of core electrons. An overview of current developments to apply DFT and TDDFT to study the key techniques of X-ray photoelectron spectroscopy, X-ray absorption spectroscopy, X-ray emission spectroscopy, and resonant inelastic X-ray scattering is presented. Insight into the accuracy that can be achieved, in conjunction with an examination of the limitations and challenges to modeling the spectroscopy of core electrons with DFT is provided.

This article is categorized under:

    Electronic Structure Theory > Ab Initio Electronic Structure Methods
    Theoretical and Physical Chemistry > Spectroscopy
    Electronic Structure Theory > Density Functional Theory

KEYWORDS

computational chemistry, density functional theory, RIXS, X-ray spectroscopy

1 | INTRODUCTION

There has been considerable advances in spectroscopic techniques that exploit X-rays, which has led to a surge in interest in their application across chemistry, physics, biology, and materials science.[1-4] These developments have been driven by the capability of modern synchrotron sources and X-ray free-electron lasers that can provide increased resolution and intensity coupled with the potential to probe processes on an ultrafast timescale.[5-7] In the future it is likely that stable and intense table-top X-ray sources will become available that will further increase the accessibility of X-ray techniques.[8,9] The key advantages of spectroscopy with X-rays arise from the localized nature of core orbitals which make them particularly sensitive to the local chemical environment. Furthermore, the large

difference in the energies of the core orbitals of different elements makes the techniques element specific, and the lifetime of core-excited states can be utilized to investigate chemical processes on an ultrafast timescale.[10]

The term X-ray spectroscopy encompasses many different techniques, including X-ray photoelectron spectroscopy (XPS), X-ray absorption spectroscopy (XAS), X-ray emission spectroscopy (XES), and resonant inelastic X-ray scattering (RIXS). These different techniques can provide information on different aspects of molecular and electronic structure. For example, XAS and XES probe the unoccupied and occupied orbitals, respectively, while XPS is sensitive to chemical bonding. Alongside the developments in the experimental measurements of X-ray spectroscopy, there has been an intense effort toward accurately simulating the spectra. This synergy between experiment and theory is critical since modeling often proves to be an essential component in the analysis and interpretation of the experimental data. The simulation of X-ray spectroscopy presents a number of challenges to theory. Chemistry is largely concerned with the properties of valence electrons and quantum chemical methods have been developed within this context, and as a consequence the accurate description of core electrons has been a lower priority, resulting in the methods not being optimal to treat X-ray spectroscopies. It is also necessary to be able to describe the variety of different spectroscopic techniques coupled with the study of heavier elements where excitations from different shells, such as the K-edge and L-edge, are important and relativistic effects become more prominent. Furthermore, in some cases it is possible to exploit the distinctive properties of core orbitals to increase the computational efficiency of the calculations.

Within quantum chemistry it is possible to model X-ray spectroscopy through wavefunction-based methods or density functional theory (DFT).[11-13] Wavefunction based methods have the advantage that it is well understood how the calculations can be systematically improved, and in recent years developments in the algebraic construction method,[14-19] coupled cluster theory[20-25] and multi-configurational wavefunction approaches[26-28] have transformed what can be achieved in the application of wavefunction based methods to simulate X-ray spectroscopy. The primary advantage of DFT is that it typically has a lower computational cost than wavefunction based methods. X-ray spectroscopy has a very diverse range of applications, which can involve surfaces, biological systems, liquids, and materials. A common theme between these applications is that they involve large and complex systems that are more accessible to DFT calculations. However, the use of an approximate treatment of the exchange–correlation term can lead to errors and the potential for inaccurate spectra. Despite these challenges, DFT has been applied successfully in many X-ray spectroscopic studies. In this Advanced Review we will explore the different approaches and strategies within DFT for the modeling of XPS, XAS, and XES, in addition to more advanced techniques such as RIXS, highlighting the relative advantages and limitations of the computational methods, and providing an assessment of their accuracy.

2 | X-RAY PHOTOELECTRON SPECTROSCOPY

XPS is a powerful analytical technique that is widely used to probe the chemical and electronic state of molecular systems, chemical composition, and materials. From the perspective of theory, the key quantities required to simulate an X-ray photoelectron spectrum are the ionization energies of the core electrons, often referred to as the core–electron binding energies. The simplest approach to determining core-ionization energies is to apply Koopmans' theorem[29] within the context of DFT wherein the ionization energy is simply the negative of the Kohn–Sham orbital energies. This approach is widely used, although it has been shown that Koopmans' theorem does not hold for Kohn–Sham eigenvalues.[30] The major limitation of this approximation is that it neglects final state effects, that is it does not account for the relaxation of the electron density that occurs in the core-ionized state. The neglect of these effects can be significant and can potentially lead to a reordering of the core-ionization energies. Final state effects can be described fully by performing a separate calculation for the core-ionized state by invoking some procedure to prevent the variational collapse to the ground state of the cation during the self-consistent field (SCF) optimization. The ionization energy can then be simply evaluated as the difference between the ground state and core-ionized state energies in what is usually referred to as a ΔSCF method. This approach originated in the work of Bagus and Schaefer,[31] and more recently it has been implemented and developed further with an emphasis on preventing variational collapse in difficult cases.[32-37] This approach is used widely, and many applications have been reported.[38-45] The primary limitations of this approach are that a separate calculation is required for each state which can lead to many additional calculations for large systems, and it can be problematic to converge the SCF calculation for the desired core-ionized state in some cases.

2.1 | Dependence on the exchange–correlation functional

In principle, the ΔSCF approach can be applied in conjunction with any SCF based quantum chemical method. For DFT-based calculations the calculated core-ionization energies are sensitive to the choice of exchange–correlation functional, and studies comparing a range of functionals have been reported.[46-51] For example, Takahata and Chong compared a wide range of functionals for a large set of experimental core-ionization energies. It was found that the most accurate values were obtained from the Perdew–Wang (PW86 exchange and PW91 correlation) functionals with a mean absolute deviation (MAD) of 0.16 eV.[47] The PBE0 functional has demonstrated good performance in the study of amino acids[50] and the strongly constrained and appropriately normalized functional (SCAN) performed well in an extensive study considering over 100 molecules.[51] The majority of this work has focused on the elements boron to fluorine, and some care is needed since conclusions made based upon these systems may not necessarily apply for heavier nuclei.[52] It is common to assess the accuracy of the different functionals through a comparison with experimental data. A broad and balanced assessment that includes ionization of the nuclei of elements across the periodic table can be limited by the availability of high-quality experimental data for gas phase molecules. An additional complication is that most calculations do not include relativistic effects which become increasing significant for heavier nuclei. An alternative approach is to compare the calculated DFT core-ionization energies with those from high-level wavefunction based methods which allows a more direct comparison. This is reflected in Table 1 which shows a comparison between core-ionization energies computed with DFT methods and an equation-of-motion coupled-cluster theory based approach EOM-IP-CCSD[24,53] for a range of small molecules that spans ionization at the K-edge of carbon to fluorine and silicon

TABLE 1 Variation in the calculated core-ionization energies (in eV) for different exchange–correlation functionals with respect to EOM-IP-CCSD

Molecule	EOM-IP-CCSD[a]	B3LYP (Koopmans)	B3LYP (ΔSCF)	PW86 +PW91 (ΔSCF)	CAM-B3LYP (ΔSCF)	B2GP-PLYP (ΔSCF)
CH_4	290.78	−14.42	+0.12	+0.20	+0.01	+0.24
HCN	293.29	−14.92	+0.29	+0.22	+0.25	+0.49
NH_3	405.62	−16.80	−0.25	+0.03	−0.28	−0.11
HCN	406.98	−16.69	−0.36	−0.15	−0.36	−0.28
CH_3OH	539.44	−19.10	−0.92	−0.43	−0.88	−0.90
H_2O	539.90	−19.65	−0.59	−0.15	−0.54	−0.49
CH_3F	693.23	−22.28	−1.35	−0.72	−1.22	−1.43
HF	694.16	−23.07	−0.81	−0.27	−0.67	−0.73
SiH_4	1845.59	−46.84	−4.24	−3.99	−3.84	−2.53
SiH$_3$OH	1846.21	−46.97	−4.18	−3.98	−3.74	−2.40
PH_3	2148.24	−51.55	−4.96	−4.69	−4.52	−2.94
H_3PO	2150.59	−51.75	−4.92	−4.92	−4.39	−2.66
CH_3SH	2473.68	−56.03	−5.81	−5.48	−5.31	−3.60
H_2S	2474.17	−56.19	−5.54	−5.24	−5.05	−3.28
CH_3Cl	2822.93	−60.71	−6.33	−5.99	−5.77	−3.92
HCl	2823.77	−61.00	−5.94	−5.66	−5.39	−3.44
MAD	–	36.12	2.91	2.63	2.64	1.84
MAD (C-F)	–	18.35	0.60	0.29	0.55	0.60
MAD (Si-Cl)	–	53.88	5.24	4.99	4.75	3.09

Notes: The cc-pCVTZ basis set is used for the element being ionized with the cc-pVTZ basis set for the other elements. The site of the core-hole is indicated by bold font. The structures are optimized using B3LYP/6-311G**.

Abbreviation: MAD, mean absolute deviation.

[a]The EOM-IP-CCSD calculations use the core-valence separation approach and have a frozen core orbital, for further details see reference 24.

to chlorine nuclei. The calculations have been performed with the cc-pCVTZ basis set for the element that is being ionized, with the cc-pVTZ basis set used for the remaining elements. This basis set has been shown to provide core-ionization energies that are close to the basis set converged values.[52] The functionals used have been chosen to represent different general classes of functional. B3LYP[54] is a standard hybrid functional, PW86(exchange) + PW91(correlation) has previously been shown to perform well for core-ionization energies,[47] CAM-B3LYP[55] is a long-range corrected functional and B2GP-PLYP[56] is a double hybrid functional.

The core-ionization energies determined from the B3LYP Kohn–Sham eigenvalues (Koopmans′ theorem) are considerably lower than the EOM-IP-CCSD values, reflecting errors in the functional and the neglect of core-relaxation. The magnitude of these errors increases with the nuclear charge of the core-ionized nuclei. The ΔSCF approach corrects these deficiencies and shows a much closer agreement with the reference values, and for the B3LYP functional a MAD of 2.91 eV is obtained. However, it is clear that a much better performance is observed for the lighter nuclei (C-F) compared with the heavier nuclei (Si-Cl). There is a notable improvement for the PW86 + PW91 functional consistent with the work of Chong,[46,47] although the poor performance for the heavier nuclei remains. The long-range corrected functional CAM-B3LYP shows an improvement relative to B3LYP, and the MAD of 2.64 eV is very similar to PW86 + PW91. For the double hybrid there is reduction in the MAD to 1.84 eV which arises largely from an improved accuracy for the core-ionization energies of the heavier nuclei. Overall, the combination of PW86 + PW91 shows a high level of accuracy for the lighter elements, but this level of accuracy is not maintained for the heavier nuclei, and for the core-ionization energies of these nuclei the double hybrid functional shows the greatest level of accuracy.

2.2 | Dependence on the basis set

The quality of the basis set is another important factor in the calculation of core-ionization energies. An extensive survey of a large number of basis sets demonstrated that there is a slow convergence of the calculated core-ionization energies with respect to the size of the basis set, and this is particularly acute for the ionization of heavier atoms.[52] The reason for this can be attributed to smaller basis sets not having the flexibility to describe the more compact electron density of the core-ionized state, leading to an unbalanced treatment of the ground and core-ionized states.[57] Several different strategies have emerged to design moderately sized basis sets that can reproduce core-ionization energies that are consistent with the basis set converged values. These include uncontracting the basis functions,[33,58] augmenting the basis set with basis functions from the element with one greater nuclear charge (denoted Z + 1 basis sets),[57] basis sets optimized for properties related to core-excitations (denoted pcX-1 and pcX-2),[59] specifically optimized small basis sets,[60] and multiwavelet formalisms.[45]

Table 2 shows a comparison of the performance of various strategies for the core-ionization energies computed using the ΔSCF technique with the PW86 + PW91 functional. Values are computed for cc-pCVTZ (cc-pCVTZ for the element being ionized and cc-pVTZ for the remaining elements), 6−311G**, u6−311G** (6−311G** with the core basis function uncontracted), (Z+1)6−311G** (the basis set for the element being ionized augmented with basis functions for the element with one greater nuclear charge), pcX-1, and IGLO-II[61] which has been shown to perform well for the calculation of core electron properties.[62-64] The results show that there is a significant error for the 6−311G** basis set, including an unusually poor performance for the chlorine K-edge. Uncontracting the core orbital does lead to a reduction in the error, but its MAD does not reflect its general performance since it does not correct the chlorine K-edge values. The remaining three approaches all provide values that are close to those for the larger basis set across all of the molecules considered. This demonstrates that with the correct choice of basis set it is possible to achieve core-ionization energies near the basis set limit with moderately sized basis sets.

2.3 | Other approaches to determining core-ionization energies

The proceeding sections have discussed how core-ionization energies can be determined reliably using DFT with the ΔSCF approach. However, there are a wide variety of alternative approaches to determining core-ionization energies within a DFT framework. This might lead to the question of why it is necessary to consider alternative approaches to ΔSCF. One of the reasons for the need for alternative approaches is that the ΔSCF approach can be cumbersome to apply. For example, to interpret the XPS spectrum for a large organic molecule at the carbon K-edge will require a large number of separate calculations for all of the different final states. In principle, all of these need to be examined to

TABLE 2 Variation in the calculated core-ionization energies (in eV) for different basis sets, see text for details

Molecule	cc-pCVTZ	6−311G**	u6−311G**	(Z + 1)6−311G**	pcX-1	IGLO-II
CH_4	290.98	+0.29	+0.09	−0.04	−0.03	+0.02
HCN	293.51	+0.28	+0.10	−0.03	−0.04	+0.05
NH_3	405.65	+0.31	+0.04	−0.06	−0.13	+0.02
HCN	406.83	+0.43	+0.12	−0.05	−0.03	+0.05
CH_3OH	539.01	+0.37	+0.01	−0.17	−0.17	−0.03
H_2O	539.75	+0.34	−0.05	−0.15	−0.23	−0.04
CH_3F	692.51	+0.44	−0.04	−0.28	−0.18	−0.06
HF	693.89	+0.40	−0.08	−0.28	−0.26	−0.06
SiH_4	1841.60	+0.65	+0.50	−0.14	−0.11	+0.08
SiH_3OH	1842.23	+0.72	+0.57	−0.06	−0.06	+0.11
PH_3	2143.55	+0.53	+0.40	−0.09	−0.08	+0.18
H_3PO	2145.67	+0.78	+0.65	+0.20	+0.14	+0.32
CH_3SH	2468.20	+0.84	+0.71	−0.08	−0.09	+0.19
H_2S	2468.93	+0.83	+0.70	−0.09	−0.12	+0.20
CH_3Cl	2816.94	+8.65	+8.51	−0.09	−0.13	+0.19
HCl	2818.11	+8.67	+8.53	−0.11	−0.17	+0.19
MAD	–	1.53	1.32	0.12	0.12	0.11

Notes: The site of the core-hole is indicated by bold font. The structures are optimized using B3LYP/6-311G**.
Abbreviation: MAD, mean absolute deviation.

TABLE 3 Calculated carbon core-level energy shifts (in eV) relative to CH_4 for different methods using the IGLO-II basis set and PW86+PW91 functional

Molecule	ΔSCF	$-\varepsilon_i^{KS}$	$-\varepsilon_i^{HF}$	Z + 1
CH_4	0	0	0	0
CH_3OH	+1.51	+1.52	+1.74	+1.51
CH_3Cl	+1.51	+2.07	+2.20	+1.48
CS_2	+2.23	+3.61	+5.35	+1.90
HCN	+2.48	+1.80	+2.16	+2.17
CH_3F	+2.56	+2.37	+2.72	+2.54
HCONH$_2$	+3.21	+3.08	+4.08	+3.14
HCOOH	+4.51	+4.11	+5.17	+4.37
CO_2	+6.33	+5.24	+7.00	+6.12
MAD[a]	–	0.56	0.84	0.14

Notes: The site of the core-hole is indicated by bold font.
Abbreviation: MAD, mean absolute deviation with respect to ΔSCF.
[a]The structures are optimized using B3LYP/6−311G**.

check that the SCF procedure has successfully converged to the correct final state. The challenge for alternative methods is how to incorporate the final state effects without explicitly optimizing the electronic structure of each state. Another important consideration is that in interpreting XPS spectra, it is often only necessary to determine the relative energies of the core-levels, so-called core-energy shifts.

In the Z + 1 approximation, the core-ionized state is described by the system where the core-ionized atom is replaced by the valence ionized atom with one greater nuclear charge.[65] This approach has been shown to be successful in predicted the core-level energy shifts, and studies detailing comparison with ΔSCF calculations have been reported.[66-68] Table 3 shows computed core-level shifts for the carbon atom in a range of chemical environments and compares the core-level shifts determined from the Kohn–Sham ($-\varepsilon_i^{KS}$) and Hartree–Fock ($-\varepsilon_i^{HF}$) eigenvalues and the Z + 1

approximation with those from ΔSCF. The results show that both Kohn–Sham and Hartree–Fock eigenvalues do not predict the correct order of core-level shifts, with a MAD of 0.56 eV for the DFT calculations. In contrast the $Z + 1$ approximation does predict the correct order (with the exception of CH_3OH and CH_3Cl which are very close in energy) with a MAD of 0.14 eV. This is consistent with previous findings that have highlighted the merits of the $Z + 1$ approach.[68]

A more formal approach is the *GW* formalism of Hedin.[69] In the *GW* approach, many body effects beyond the mean field description of the electron–electron interaction are included via the self-energy.[70] The response of the system to the core-hole is expressed through perturbation theory and so an SCF optimization of the core-hole state is not required. In *GW* approaches, quasi-particles are introduced that have a well-defined physical meaning, and for occupied states the quasi-particle energies represent ionization potentials. There are several variants of *GW* theory based upon different approximations that reduce the computational cost. Studies assessing the accuracy of these different approximations for the calculation of core-ionization energies have been reported.[71,72]

2.4 | Simulation of X-ray photoelectron spectra

In order to simulate an X-ray photoelectron spectrum, it is necessary to have some estimation of the intensity associated with the different core ionizations. The most common approach is to assign a uniform intensity for all core orbitals which are convoluted with Gaussian or Lorentzian functions to produce a spectrum. Going beyond this most basic description of the intensity leads to the introduction of Dyson orbitals. For an ionization process the Dyson orbital is defined as the overlap between the initial *N* electron state and the final state with *N-1* electrons.

$$\varphi_{IF}^{Dyson} = \int \Psi_I^{*N}(\mathbf{x}_1, \mathbf{x}_2, ..., \mathbf{x}_N) \Psi_F^{*N-1}(\mathbf{x}_2, ..., \mathbf{x}_N) d\mathbf{x}_2, ..., d\mathbf{x}_N \tag{1}$$

A recent article has explored the properties of Dyson orbitals in detail.[73] The spectral intensity of an ionization process can be obtained from the Dyson orbitals through the following

$$P_{IF} = \int \left| \varphi_{IF}^{Dyson}(\mathbf{x}) \right|^2 d\mathbf{x} \tag{2}$$

and this has been implemented within quantum chemical calculations.[24] For photoelectron spectroscopy of valence orbitals, the band intensities can be shown to be dependent on the photon energy.[74] This energy dependence can be captured by the Gelius model[75] which considers the photoionization cross-section for a molecular orbital to be a sum of atomic orbital contributions for which energy dependent cross-sections are available. By their nature, the core orbitals of a given nuclei are much more uniform throughout a system which makes the impact of a Dyson orbital description and the dependence on photon energy less important, and in most cases assuming a uniform intensity is satisfactory.

3 | X-RAY ABSORPTION SPECTROSCOPY

X-ray absorption spectra are rich with information and comprise two different components. The structure near the absorption edge arises from the excitation of core electrons to low-lying orbitals to give a bound state below the ionization threshold. This region of the spectra is commonly referred to near-edge X-ray absorption fine structure (NEXAFS). The region at higher energies, typically beyond 20 eV of the absorption edge, is referred to as extended X-ray absorption fine structure (EXAFS) and is characterized by weak oscillations that arise from the scattering of the photoelectron by its environment. Historically, NEXAFS was often associated with surface science where technique could be applied to probe the orientation and bonding of adsorbed molecules.[76] More recently, XAS has been used to probe the structure of liquids, such as water and methanol,[63,77-79] explore the nature of active sites in metalloproteins[80] and monitor the breaking of a chemical bond.[81]

In principle it would be possible to simulate X-ray absorption spectra with a ΔSCF approach,[33] and orthogonality constrained DFT has been applied to core excitations.[82] However, approaches that explicitly consider each state can become impractical owing to the large number of states that can be required to simulate an X-ray absorption spectrum

even for a moderately sized molecule. A number of different methods have been developed with the aim of providing reliable X-ray absorption spectra with a relatively low computational cost. An early approach was the direct static exchange (STEX) method.[83] The limitations of this approach were the neglect of electron correlation and the independent channel approximation, and addressing these deficiencies led to the transition potential method.[84,85] DFT in conjunction with the transition potential method (TP-DFT) has been used widely to simulate X-ray absorption spectra. The key aspect of TP-DFT is that it introduces a fractional occupancy of the core-orbital. Typically, a fractional occupancy of 0.5 is used which is suitable for core-excitations since it provides a balance between initial and final state effects.[85] Another method that goes beyond the STEX approximation through the inclusion of the coupling between non-orthogonal configurations is non-orthogonal configuration interaction singles (NOCIS).[86,87] Prendergast and co-workers have developed the excited electron and core-hole approach (XCH) which models the first core-excited state by representing the core-excited atom using a modified pseudopotential, and the electron excited from this atom is placed in the first available valence orbital.[88-91] In this approach, the core-excited state becomes effectively the ground state of the system and be treated with standard Kohn–Sham DFT methods allowing large systems to be studied. X-ray absorption spectra have also been simulated based upon the Bethe–Salpether equation (BSE).[92-94] This approach treats particle-hole interactions and includes a self-energy based upon the *GW* approximation. Efficient implementations to solve the BSE have been reported,[95] and the approach has been used to study many systems.[96-98]

Linear response time-dependent density functional theory (TDDFT) has become established as one of the most popular methods for simulating X-ray absorption spectra, and a detailed review comparing TDDFT and BSE methods is available.[99] More specifically TDDFT is suitable for describing the NEXAFS region, although extensions to study the higher energy region have been reported.[100,101] In these calculations, it is common to invoke the Tamm–Dancoff approximation[102] where the following equation is solved

$$\boldsymbol{A}\mathbf{X} = \omega\mathbf{X} \tag{3}$$

where

$$A_{ia,jb} = \delta_{ij}\delta_{ab}(\epsilon_a - \epsilon_i) + (ia|jb) + (ia|f_{XC}|jb) \tag{4}$$

$$(ia|jb) = \int\int \psi_i^*(\mathbf{r}_1)\psi_a(\mathbf{r}_1)\frac{1}{r_{12}}\psi_j^*(\mathbf{r}_2)\psi_b(\mathbf{r}_2)d\mathbf{r}_1 d\mathbf{r}_2 \tag{5}$$

$$\left(ia\middle|f_{XC}|jb\right) = \int\int \psi_i^*(\mathbf{r}_1)\psi_a(\mathbf{r}_1)\frac{\delta^2 E_{XC}}{\delta\rho(\mathbf{r}_1)\delta\rho(\mathbf{r}_2)}\psi_j^*(\mathbf{r}_2)\psi_b(\mathbf{r}_2)d\mathbf{r}_1 d\mathbf{r}_2 \tag{6}$$

and ϵ_i are the orbital energies and E_{XC} is the exchange–correlation functional. One issue that needs to be addressed when applying TDDFT to study core excitations is that these excitations lie very high in the excitation manifold. Stener and co-workers showed that problem could be addressed by simply restricting the occupied orbital space (i,j) to include only the relevant core orbitals, this is often referred to as a restricted excitation window (REW) approach.[103] This approximation is similar to the core-valence separation scheme (CVS).[104] Alternative approaches include a projection method that allows transitions within a specified energy range to be determined,[105] and the resonant converged complex polarization propagator approach of Norman and co-workers.[106,107] The application of TDDFT to study X-ray absorption spectroscopy is very diverse considering both K-edge and L-edge spectra, and illustrative examples include biological systems,[108-110] metal complexes,[111] radicals,[112] molecules on surfaces,[113,114] ionic liquids,[115] liquid water,[63,64] lanthanide complexes,[116,117] and vibrationally resolved spectra.[118]

While TDDFT is computational less demanding than methods such as EOM-CCSD, it can become challenging to study X-ray absorption spectra for large systems. The high density of core-excited states makes simulating spectra in the NEXAFS region more computationally expensive than a comparable calculation of the UV/vis spectra. This is particularly the case when excitations from many core-orbitals are required, which is often the situation when studying the carbon K-edge of organic molecules. There are two aspects to the computational cost, firstly the CPU time required and secondly the memory required. The first of these arises from the large number of integrals required in the construction of the matrix **A** (Equation 4) and can often be overcome with a degree of patience coupled with effective parallelization,

and it is the memory required that can often be the limiting factor for calculations. Most TDDFT codes use the Davidson algorithm[119] which is an iterative subspace approach. For a given root k, the eigenvector is expanded as[120]

$$\mathbf{X}^k \approx \mathbf{x}^k = \sum_i^L c_i^k \mathbf{b}_i \qquad (7)$$

where $\mathbf{x}^k$ is the current approximation to $\mathbf{X}^k$. On each iteration if the root is not converged a correction vector is added to the subspace

$$\mathbf{X}^k = \mathbf{x}^k + \boldsymbol{\delta}^k \qquad (8)$$

and orthogonalized with respect to the existing subspace. This necessitates all of the subspace vectors to be retained and corresponds to L vectors of length $n_{occ} \times n_{virt}$, where n_{occ} is the number of occupied orbitals and n_{virt} is the number of virtual orbitals. Methods that simply project unwanted excitations from the subspace reduce the cost of the calculations in terms of the number of roots required to access the high energy region, but do not reduce n_{occ} or n_{virt}.

The high memory demands associated with the Davidson approach are avoided in real time TDDFT,[121] which has been applied to the study of core-excitation spectra.[122] In these approaches the density matrix is propagated in time, and for core excitations very small time steps can be required to avoid sampling errors in conjunction with long simulations to ensure convergence. Other work has explored exploiting the nature of core-excitations to optimize the efficiency of the calculations within the Davidson framework, and this work has focused on the K-edge.[123,124] One strategy that has been adopted is to use severe integral screening thresholds coupled with reduced quality integration grids for the TDDFT part of the calculation. This has been shown to reduce the CPU time significantly with only a small effect on the calculated spectra,[123] and is particularly effective for the K-edge of transition metal complexes.[124] The memory requirements can be reduced by forming **A** explicitly in the core-excitation space. This can be reduced further by imposing additional restrictions on the size of the virtual orbital space (n_{virt}) which represents an example of restricted subspace TDDFT[125] and this strategy has been used in the simulation of the K-edge absorption spectra of fullerenes[124] and RIXS simulations.[126,127]

The effectiveness of these approaches is illustrated in Figure 1 which shows the calculated NEXAFS spectra for a set of polyaromatic hydrocarbon (PAH) molecules and compares a standard TDDFT calculation with modified TDDFT[124] where increased integral screening and reduced quality integration grid coupled with a restricted virtual orbital space. These calculations include the lowest 50 states at the carbon K-edge and use the SRC1r1 functional.[128] The study of PAHs represents a challenging case for TDDFT since it requires excitations to be included from a large number of core orbitals which results in a large number of excited states being needed to simulate the spectra. The spectra for the modified TDDFT accurately reproduce those for the standard TDDFT calculation. Some differences are evident, such as the higher energy band for naphthalene and the intensities of some of the bands in pentacene. These changes arise primarily from the truncation of the virtual orbital subspace, and this approximation needs to be used with some care. Overall, these errors are within the size of the typical errors associated with TDDFT calculations. The benefit of these approximations become evident when considering the time for the calculations and the memory required to store the subspace vectors. The time for the calculations is reduced by approximately a factor of four, and this reduction in time depends on the balance between the number of atoms being core-excited and the total number of atoms in the molecule. In this regard, the study of PAH molecules represents the lower end of potential speed up in the calculations. The storage required is also reduced significantly. The extent of these savings this increase with the size of the PAH molecule, and for pentacene the storage required is reduced by a factor of about seven.

The above discussion has focused on the K-edge of molecular systems. The attraction of studying the K-edge is its relative simplicity. For heavier elements the L-edge is energetically more accessible, and for transition metal complexes 2p → d transitions are dipole allowed making the technique more suitable for probing partially filled d shells. However, the simulation of L-edge spectra is complicated by the spin-orbit coupling effects associated with the 2p core-hole which leads to L_2 and L_3 edges. The reader is referred to a recent review[129] for a thorough overview of quantum chemical calculations of L-edge spectra that includes TDDFT methods. It is possible to treat these spin-orbit effects for TDDFT using the zero-order regular approximation (ZORA)[130,131] in addition to perturbative treatments with multi-configurational wavefunction methods[132,133] and the DFT/ROCIS method.[134,135] These more approximate approaches becomes less suitable for heavier elements and recently linear response exact two-component relativistic TDDFT has been reported.[136] Beyond linear response TDDFT,

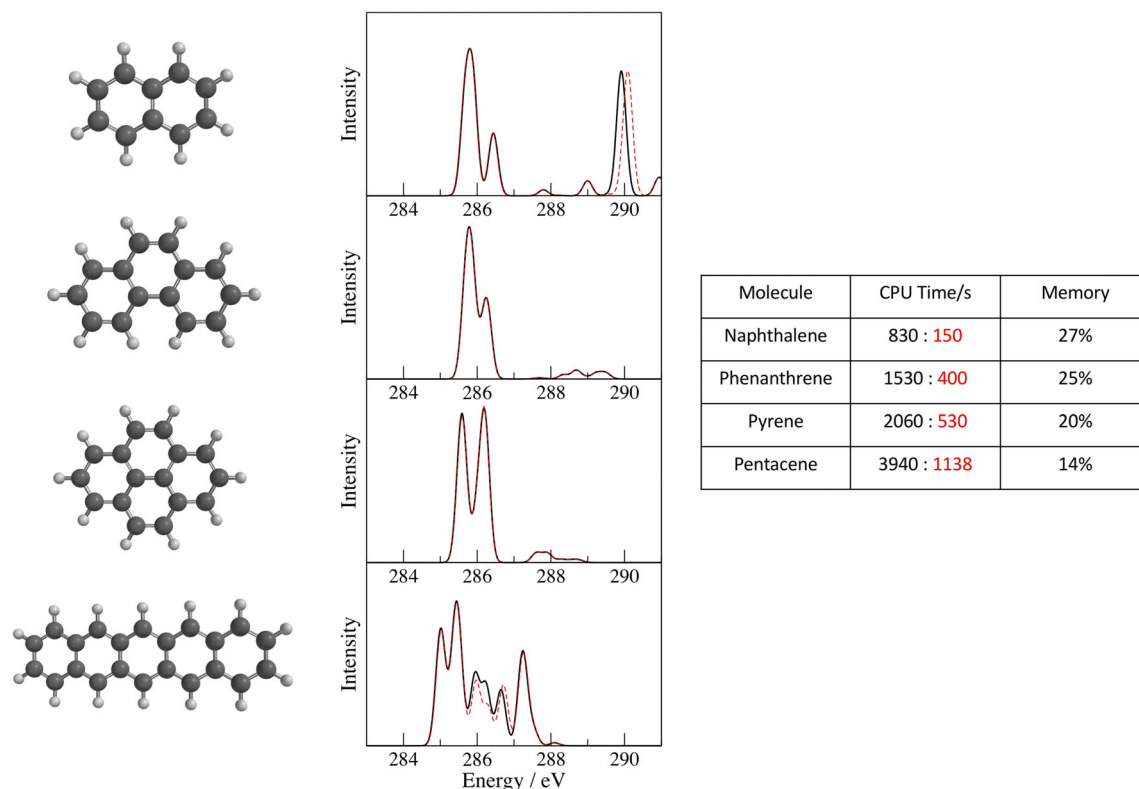| Molecule	CPU Time/s	Memory
Naphthalene	830 : 150	27%
Phenanthrene	1530 : 400	25%
Pyrene	2060 : 530	20%
Pentacene	3940 : 1138	14%

FIGURE 1 Comparison of standard TDDFT (black line) with fast-low memory TDDFT where the virtual space is limited to the lowest 50 orbitals (red line) for the calculation of the lowest 50 states to naphthalene, phenanthrene, pyrene and pentacene. The CPU time reflects the time for the TDDFT calculation. The memory represents the fraction of the storage required for the subspace vectors for the modified calculation compared with the standard calculation. The structures are optimized using B3LYP/6−311G**

relativistic 4-component real-time TDDFT[137] and damped 4-component DFT[138] formalisms have been applied to the study of $L_{2,3}$ edges.

3.1 | Dependence on the exchange–correlation functional

The exchange–correlation functional plays a critical role in the accuracy of TDDFT calculations of X-ray absorption spectra. Calculated core-excitation energies at the K-edge with standard functionals underestimate the experimentally measured values, even when relativistic effects are taken into account.[128,139,140] The magnitude of this underestimation is greater for generalized gradient corrected (GGA) functionals compared with hybrid functionals and increases with the nuclear charge of the excited nuclei. For example, for a hybrid functional the error ranges from 11 eV for the carbon K-edge to over 100 eV for the copper K-edge. This error has been associated with the self-interaction error and highlights how this error manifests itself in the description of core electrons.[128,141,142] Different strategies have emerged to correct for this error. The first approach has been to exploit the fact that this error is systematic and can be corrected by applying a uniform energy shift to the calculated spectrum. This shift can also account for relativistic effects making it unnecessary to explicitly account for these effects. In this approach the computed spectrum is shifted such that the lowest peak is aligned with experiment[143,144] or this shift can be determined in a separate ΔSCF calculation. It then becomes important for the functional to predict the relative position of the bands correctly. Several studies have assessed the performance of a variety of exchange–correlation functionals in this regard.[144,145] Lestrange et al.[145] studied the performance of six commonly used functionals including B3LYP, BHandHLYP, and HSE06 with basis sets of varying quality for 30 different transitions from gas-phase experiments at the C, N, and O K-edges. The performance of the different hybrid functionals was similar, with HSE06 showing the lowest errors. More recently, a large set of $1s \rightarrow \pi^*$ transitions were used to assess different exchange–correlation functionals relative to transition energies calculated with EOM-CCSD and ADC methodologies.[146] This study also focuses on the C, N, and O K-edges and showed

good performance of long-range corrected functionals compared with standard hybrid functionals. This work assessing the performance of functionals has only considered excitations at the K-edge of relatively light nuclei and it has not been determined whether the findings also apply to excitations at the K-edge of heavier nuclei.

An alternative strategy is to construct functionals that are able to predict core-excitation energies without the need to apply an energy shift to the calculated spectra. This is possible through modifying the exchange component of the functional to ameliorate the self-interaction error. Nakai and co-workers developed the CVR-B3LYP functionals[139,140] that are designed to be able to treat all types of excitations, including core excitations. This was achieved by using an appropriate fraction of Hartree–Fock (HF) exchange dependent on the nature of the transition being studied. Another study increased the fraction of HF exchange within a B3LYP-like functional to 57% in a study of small hydrocarbons.[114] While this does correct the systematic underestimation of the core-excitation energies, the high fraction of HF exchange can adversely affect the relative position and intensity of the bands. A potential solution to this is to include an increased fraction of HF only in the short-range, that is, only for small $r_{12} = |\mathbf{r}_1 - \mathbf{r}_2|$, in the evaluation of the exchange-energy. In this spirit, a modification of the LCgau-BOP functional for core-excitations does include an additional contribution of HF in the short-range.[147] Another development was the introduction of short-range corrected (SRC) functionals[128] which invert the principle of long-range corrected functionals such as CAM-B3LYP[55] so that there is an increased fraction of HF in the short-range. These functionals have been parameterized for the K-edge of light elements (boron-fluorine) and heavier elements (aluminum to chlorine), and are called SRC1r1 and SRC1r2, respectively. The SRC1r2 functional has also been applied for the K-edge of first row transition metal systems.[108,148] These functionals predict transition energies within an error of approximately 0.5 eV, and also predict the relative energies of the transitions accurately.[146] The CAM-QTP(01) is range-separated functional with 100% HF exchange in the long range the functional is parameterized so that the Kohn–Sham eigenvalues are approximately equal to the vertical ionization energies.[149] This functional has been applied to core-excitations and shown to be in agreement with experiment without the need for an applied energy shift.[150]

3.2 | Time-resolved X-ray absorption spectroscopy

The emergence of third generation synchrotron sources and X-ray free electron lasers have made time-resolved X-ray absorption spectroscopy (TR-XAS) studies possible. This has allowed complex processes that occur on a fast-timescale to be probed.[7,151,152] The study of TR-XAS requires a combination of molecular dynamics simulations on the excited state potential energy surface with the calculation of X-ray absorption spectra for a system in an electronically excited state. Simulations of this nature have been reported based upon coupled cluster based methods[153] and multi-reference wavefunction methods.[154] Early simulations of TR-XAS using TDDFT in conjunction with the multi-configuration time-dependent Hartree (MCTDH) method were reported by Penfold et al.[155,156] Other examples of the simulation of TR-XAS using TDDFT have been reported by Leone and co-workers[157] and include the study of an electrocyclic ring-opening reaction.[158] In these studies, the X-ray absorption spectrum for an excited state is determined by applying TDDFT to an excited state determinant generated by the maximum overlap method (MOM),[32] in a MOM-TDDFT approach. For the quantum dynamics aspect of these simulations, the difficulty arises from the increasing dimensionality. This can be reduced by using a set of time-evolving Gaussian basis functions. With this representation a fully quantum description can be achieved, while maintaining the advantages of the classical trajectory simulations.[159,160] Within this framework, Northey et al. used the DD-vMCG method[161,162] to simulate the time-resolved XANES spectra of CF_4^+ dissociation[163] and ultrafast nonadiabatic dynamics of pyrazine probed at the nitrogen K-edge.[164] In this latter paper, two methods were used to simulate the excited state XANES spectra, multi-configurational second order perturbation theory restricted active space (RASPT2) and MOM-TDDFT. The simpler MOM-TDDFT approach captures several qualitative features of the RASPT2 simulations at much reduced computational effort. However, features such as the conical intersection where static correlation effects become important were found to require a multi-configurational treatment.

4 | X-RAY EMISSION SPECTROSCOPY

XES measures the X-ray emission following the ionization of a core electron and provides a probe of the occupied orbitals. Here we focus on XES under nonresonant conditions, that is where the intermediate state corresponds to a core-ionized molecule. The computational methods described earlier to study XPS and XAS can also be adapted to simulate XES, and these approaches differ in their computational cost, ease of use and how the relaxation of the electronic

structure in the intermediate state is treated. The computationally most simple approach to simulating an X-ray emission spectrum is to determine the transition energies as the difference between the Kohn–Sham orbital energies

$$\Delta E = \epsilon_v - \epsilon_c \tag{9}$$

with the oscillator strengths estimated using

$$f \propto \left| \langle \phi_c | \hat{\mu} | \phi_v \rangle \right|^2 \tag{10}$$

where ϕ_c is a core orbital and ϕ_v is a valence orbital. This is similar in spirit to Koopmans' theorem for XPS, and the advantages of this approach are that it only requires a Kohn–Sham DFT calculation to be performed and it is able to predict the relative energies of the experimental bands to a high level of accuracy that allow observed experimental bands to be assigned with confidence. This method has been used successfully[165,166] and allows the XES of large systems such as carbon nanotubes to be studied.[167]

Going beyond this approach requires some explicit consideration of the core-ionized state and the associated relaxation of the electronic density. This can be achieved via ΔSCF calculations, however converging SCF calculations for the large number of final states is challenging. An alternative approach is to use TDDFT where the relevant core-hole state is used as the reference determinant.[168] For these calculations the Tamm–Dancoff approximation is necessary, and the resulting negative eigenvalues correspond to the X-ray emission transitions. The electronic relaxation in the core-ionized states is captured by the reference determinant and the approach is straightforward to apply. This strategy to simulating X-ray emission spectra was originally proposed in the context of EOM-CCSD calculations,[169] and has also been adapted within ADC calculations[170] and applied with TDDFT to study organic molecules,[171,172] water,[64] and transition metal complexes.[173-177]

There have been relatively few studies that directly compare these different approaches to computing X-ray emission spectra. Mortensen et al.[175] compared the valence-to-core X-ray emission spectroscopy of zinc and iron transition metal complexes determined based upon Kohn–Sham orbital energies, full multiple scattering method implemented with FEFF code[178,179] and TDDFT. All the approaches provided a good description of the experimental spectra, but it was concluded that generally TDDFT gives better agreement with the positions and amplitudes of the spectral features. A recent study has explored the role of exchange–correlation functional and basis set on calculations of X-ray emission spectra with TDDFT based upon a set of eight organic molecules.[171] Standard hybrid or long-range corrected functionals systematically overestimate experimental emission energies, and of the functionals studied the CAM-B3LYP functional gave the best agreement with experimental spectra once a uniform energy shift was applied. This mirrors the good performance of this functional for TDDFT calculations of XAS. This study also highlights the need for large or specifically modified basis sets to achieve convergence of the calculated spectra with respect to the basis set. This is in contrast to TDDFT calculations of XAS where the quality of the basis set is less critical[52] and arises from the need to explicitly describe the core-ionized intermediate state.

A comparison between K-edge X-ray emission spectra computed based upon the Kohn–Sham eigenvalues (Equations 9 and 10) and TDDFT is shown in Figure 2. These calculations used the CAM-B3LYP exchange–correlation functional and the cc-pCVTZ basis set. For the three organic molecules, CH_3OH, NH_3 and CH_3Cl, both Kohn–Sham DFT and TDDFT provide an excellent description of the experimental spectra once an energy shift is applied, and there is little difference between the spectra evaluated by the different methods. For the transition metal complex, $Cr(CO)_6$, some notable differences do emerge. For this complex the TDDFT spectrum provides a better agreement with the experiment, while the Kohn–Sham DFT based spectrum is poorer.

4.1 | Valence to core XES of transition metal complexes

The X-ray emission spectrum of $Cr(CO)_6$ in Figure 2 is an example of a valence to core (VtoC) emission spectrum. This region of the spectrum of transition metals complexes comprises transitions from orbitals associated with the ligands. There has been considerable interest in VtoC spectra since it can contain information on the nature of the metal–ligand bonding.[184] In a study of ferrocene derivatives, it has been shown that the sensitivity of VtoC XES does not extend beyond the first coordination shell because the spectra are dominated by dipole allowed transitions from occupied ligand orbitals.[185] The structural sensitivity of VtoC XES has also been explored in the context of a structural sensitivity parameter.[186] A wealth of high quality experimental data is now available,[165,183-185,187-191] and several groups have
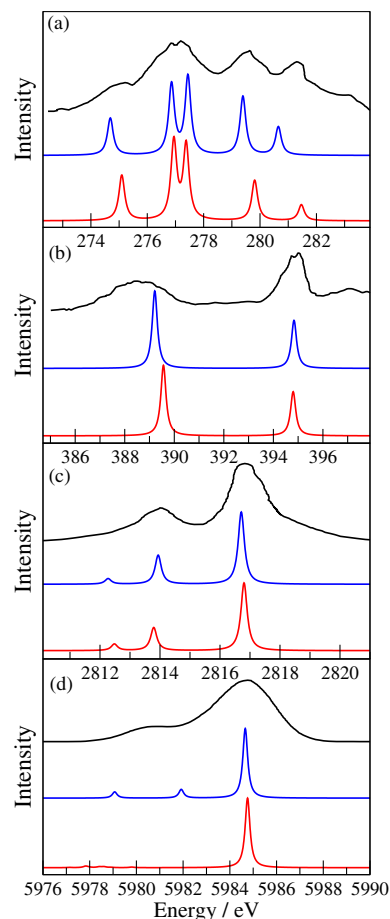
FIGURE 2 Comparison of calculated K-edge X-ray emission spectra based upon the Kohn–Sham orbital energies (red line) and TDDFT (blue line) with experiment (black line) for (a) **CH₃OH**, (b) **NH₃**, (c) **CH₃Cl** and (d) **Cr**(CO)₆ with the CAM-B3LYP functional and cc-pCVTZ basis set. The structures are optimized using B3LYP/6−311G**, except for (d) where B3LYP/6−31G* was used. Experimental data from references 180-183. The calculated spectra have been shifted to align with experiment, the following energy shifts were applied for Kohn–Sham spectra (a) +10.9 eV, (b) +13.0 eV, (c) +62.6 eV, (d) +123.5 eV and (a) −5.7 eV, (b) −7.0 eV, (c) −26.5 eV, (d) −18.3 eV for TDDFT

addressed the simulation of these spectra in detail using the DFT, for example the work of Neese and others,[165,183] and using TDDFT.[173-176,185]

It has been suggested that short-range corrected functionals performed well in the DFT simulations of these spectra,[166] and a modified TPSSh functional with 12.5% HF exchange has also been observed to perform well.[192] Figure 3 shows a comparison of Kohn–Sham DFT VtoC X-ray emission spectra calculated with two different functionals, CAM-B3LYP and SRC1r2, with experiment for the chromium K-edge of three complexes, $Cr(CO)_6$, $Cr(\eta-C_6H_6)(CO)_3$, and $Cr(\eta-C_6H_6)_2$. The data shows that the choice of functional can have a significant effect on the relative energies and intensities of the predicted emission bands. The short-range corrected functional, SRC1r2, provides an excellent description of the spectra for all three complexes, while the predicted spectra for the CAM-B3LYP functional are significantly poorer for two of the complexes. While an extensive comparison of different functionals with respect to their performance for VtoC X-ray emission spectra is not available, it is clear that a careful choice of functional can lead to an improved description of experimental data.

Another factor that has emerged as important in the simulation of these spectra is the failure of the dipole approximation (Equation 10) to adequately describe the intensities of some of the spectral bands observed in experiment. This was originally noted in a study of iron complexes by DeBeer, Neese and co-workers,[165] where the quadrupole contribution to the intensities was included. In a later work the importance of the quadrupole contribution to the intensities was also demonstrated in a study of halozincate complexes.[176] A detailed account of the mathematical formulation and working equations for an origin independent treatment of the quadrupole contribution to intensities for X-ray spectroscopy has been reported by Jacob and co-workers,[193] and the importance of these higher order contributions to the intensity will become more significant for hard X-ray studies.

5 | OTHER X-RAY SPECTROSCOPIC TECHNIQUES

In addition to XPS, XAS, and XES, there are many other X-ray spectroscopic techniques that are commonly used. These techniques include multiphoton techniques that involve more than one electronic transition. Simulating the

FIGURE 3 Comparison of calculated K-edge X-ray emission spectra based upon the Kohn–Sham orbital energies with CAM-B3LYP (red line) and SRC1r2 (blue line) functionals with experiment (black line) for (a) $Cr(CO)_6$, (b) $Cr(\eta-C_6H_6)(CO)_3$, and (c) $Cr(\eta-C_6H_6)_2$. The cc-pCVTZ basis set was used and the structures are optimized using B3LYP/6−31G*. Experimental data from reference 183. The calculated spectra have been shifted to align with experiment
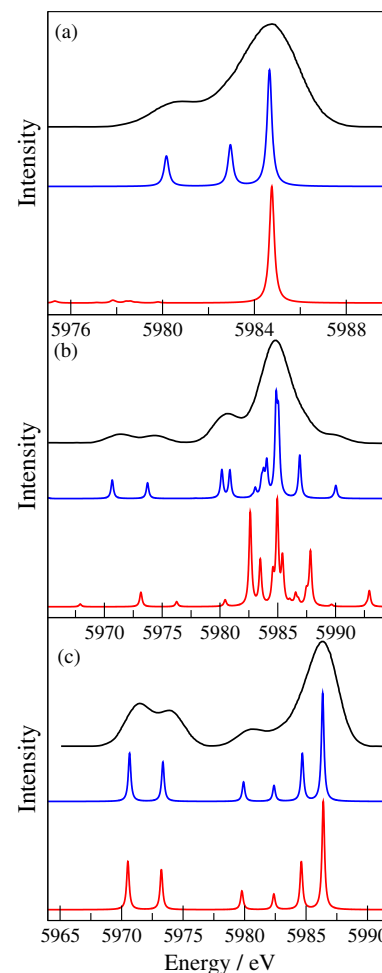
spectra for these spectroscopic methods with DFT-based methods is considerably more challenging since, for example, the adiabatic approximation limits TDDFT to describing singly excited states. However, several groups have progressed the application of DFT and TDDFT to study these more advanced spectroscopic techniques.

In Auger spectroscopy, the energy released following a transition of a valence electron to a lower energy (core) orbital leads to the excitation or ionization of another electron. The energies of the initial and final states can be determined via ΔSCF calculations.[194-196] A much more detailed picture of the Auger process is obtained by describing the process in the time domain through non-adiabatic molecular dynamics simulations allowing for surface hopping between the different states,[197] and this has been implemented within real-time TDDFT and applied to CdSe quantum dots.[198] Another type of spectroscopy that has become possible in recent years is double core-hole photoionization and the related process of simultaneous core-ionization and core excitation.[199,200] This ionization can occur on a single atom or two different atoms. DFT based approaches to have been used to determine these ionization energies[201,202] and benchmark coupled cluster theory values are available.[203]

Resonant inelastic X-ray scattering (RIXS) is a fast-developing technique wherein absorption of a photon creates a core-excited intermediate state and emission from this state leads to the final state.[204] RIXS can provide information for a range of core-excited intermediate states with the capability of probing the evolution of the nuclear and electronic structure occurring in the intermediate state within the lifetime of core-excited state. The RIXS intensity can be plotted as a function of the absorption and emission energies, in a so-called RIXS map, to provide a complete picture of the RIXS process. RIXS maps have been reported for a number of systems, including gas-phase water,[205] amino acids,[206] ammonia[207] and alcohols.[208] Quantum chemical simulations of RIXS are less well developed than those for XPS, XAS, and XES described above. The key quantities required to determine RIXS intensities are the transition energies and transition dipole moments of the excitation and emission processes, which means that simulation of RIXS maps requires both the excitation and emission processes to be described accurately.

One computational approach to interpreting RIXS maps is to treat the problem in terms of resonant X-ray emission (RXES). In this approach, X-ray emission spectra are computed for different core-excited states.[22,166,167,208-213] This can be achieved using TDDFT by using a reference determinant corresponding to the relevant core-excited state.[214] To go beyond a RXES picture it is necessary to determine the RIXS cross-sections. This can be done using the Kramers–Heisenberg (KH) formalism,[215-219] and a semiclassical approximation to the KH equation has been introduced and applied to study hydrogen bonding liquids.[220-223] There have been relatively few attempts to simulate a complete RIXS map, but studies of the gas-phase water molecule have been reported.[16,212,214] A study on the water molecule compared RIXS maps simulated based upon ADC(2)-x and TDDFT calculations of the absorption and emission processes.[214] It was shown that both methods where able to provide a qualitative description of the RIXS map. For the TDDFT calculations different functionals were used to describe the absorption and emission processes. It would be preferable to use the same functional for both absorption and emission, and CAM-B3LYP is promising in this regard. A further challenge is evident in the RIXS of the water molecule, where some of the observed features are associated with molecular dissociation that occurs in the core-excited intermediate states.[205] These effects can be incorporated into the simulations through conformational sampling of both the ground (initial) and core-excited (intermediate) states.[214] More recently, TDDFT with a restricted subspace approximation has been used to simulate the RIXS of larger molecules including 2-thiopyridone.[127] One note of caution when applying TDDFT to study these processes is that it is possible that some of the intermediate states may have multiple unpaired electrons where static correlation becomes important. TDDFT is likely to perform poorly for these states and a genuine multireference treatment may be required.[224]

6 | CONCLUSION

The growth in experimental studies exploiting the spectroscopy of core electrons to probe chemical and biological processes has fueled the demand for accurate simulations of core electron spectroscopies such as XPS, XAS, XES, and RIXS. While there has been considerable progress within the framework of wavefunction-based quantum chemical methods to this problem, the application of DFT remains an attractive option owing to its relatively low computational cost which means it can be readily applied to study quite large systems. Modern DFT has been developed largely to treat properties that are associated with valence electrons and additional considerations need to be taken into account when applying DFT to simulate spectroscopies that depend on the unique properties of core electrons. This review has demonstrated that using DFT and/or TDDFT it is possible to simulate a range of different X-ray spectroscopic techniques to a sufficiently high degree of accuracy that constitute a reliable basis to interpret and analysis experimental data. This success can often be predicated on an appropriate choice of exchange–correlational functional, and there remains more to be learned about how functionals can be improved to achieve the best performance for core–electron spectroscopies. The explicit treatment of relativistic effects is also can important consideration to achieve higher levels of accuracy, particularly for the L and M-edges. The future holds considerable promise to advance these simulations further, methods that move from a static to dynamic picture of the electronic structure and capture the evolution of the system in core-excited states including surface hopping represent one area where valuable progress can be made.

CONFLICT OF INTEREST
The author has declared no conflicts of interest for this article.

DATA AVAILABILITY STATEMENT
The data that support the findings of this study are available from the corresponding author upon reasonable request.

ORCID
Nicholas A. Besley https://orcid.org/0000-0003-1011-6675

RELATED WIREs ARTICLES
Theoretical X-ray spectroscopy of transition metal compounds

REFERENCES

1. Öström H, Öberg H, Xin H, LaRue J, Beye M, Dell'Angela M, et al. Probing the transition state region in catalytic CO oxidation on Ru. *Science*. 2015;*347*:978–82.

2. Lancaster KM, Roemelt M, Ettenhuber P, Hu Y, Ribbe MW, Neese F, et al. X-ray emission spectroscopy evidences a central carbon in the nitrogenase iron-molybdenum cofactor. *Science*. 2011;*334*:974–7.

3. Buzzi M, Först M, Mankowsky R, Cavalleri A. Probing dynamics in quantum materials with femtosecond X-rays. *Nat Rev Mater*. 2018;*3*:299–31.

4. Bokarev SI, Kühn O. Theoretical X-ray spectroscopy of transition metal compounds. *WIREs Comput Mol Sci*. 2019;*10*:e1433.

5. Chergui M, Collet E. Photoinduced structural dynamics of molecular systems mapped by time-resolved X-ray methods. *Chem Rev*. 2017;*117*:11025–65.

6. Schoenlein R, Elsaesser T, Holldack K, Huang Z, Kapteyn H, Murnane M, et al. Recent advances in ultrafast X-ray sources. *Philos Trans R Soc A*. 2019;*377*:20180384.

7. Milne CJ, Penfold TJ, Chergui M. Recent experimental and theoretical developments in time-resolved X-ray spectroscopies. *Coord Chem Rev*. 2014;*278*:44–68.

8. Seidler GT, Mortensen DR, Remesnik AJ, Pacold JI, Ball NA, Barry N, et al. A laboratory-based hard X-ray monochromator for high-resolution X-ray emission spectroscopy and X-ray absorption near edge structure measurements. *Rev Sci Instrum*. 2014;*85*:113906.

9. Chen M-C, Arpin P, Popmintchev T, Gerrity M, Zhang B, Seaberg M, et al. Bright, coherent, ultrafast soft X-ray harmonics spanning the water window from a tabletop light source. *Phys Rev Lett*. 2010;*105*:173901.

10. Piancastelli MN, Goldsztejn G, Marchenko T, Guillemin R, Kushawaha RK, Journel L, et al. Core-hole-clock spectroscopies in the tender X-ray domain. *J Phys B*. 2014;*47*:124031.

11. Norman P, Dreuw A. Simulating X-ray spectroscopies and calculating core-excited states of molecules. *Chem Rev*. 2018;*118*:7208–48.

12. Besley NA, Asmuruf FA. Time-dependent density functional theory calculations of the spectroscopy of core electrons. *Phys Chem Chem Phys*. 2010;*12*:12024–39.

13. Besley NA. Density functional theory based methods for the calculation of X-ray spectroscopy. *Acc Chem Res*. 2020;*53*:1306–15.

14. Schirmer J, Trofimov AB, Randall KJ, Feldhaus J, Bradshaw AM, Ma Y, et al. K-shell excitation of the water, ammonia, and methane molecules using high-resolution photoabsorption spectroscopy. *Phys Rev A*. 1993;*47*:1136–47.

15. Köppel H, Gadea FX, Klatt G, Schirmer J, Cederbaum LS. Multistate vibronic coupling effects in the K-shell excitation spectrum of ethylene: symmetry breaking and core-hole localization. *J Chem Phys*. 1997;*106*:4415–29.

16. Trofimov AB, Moskovskaya T, Gromov EV, Vitkovskaya NM, Schirmer J. Core-level electronic spectra in ADC(2) approximation for polarization propagator: carbon monoxide and nitrogen molecules. *J Struct Chem*. 2000;*41*:483–94.

17. Wenzel J, Wormit M, Dreuw A. Calculating core-level excitations and X-ray absorption spectra of medium-sized closed-shell molecules with the algebraic-diagrammatic construction scheme for the polarization propagator. *J Comput Chem*. 2014;*35*:1900–15.

18. Wenzel J, Wormit M, Dreuw A. Calculating X-ray absorption spectra of open-shell molecules with the unrestricted algebraic-diagrammatic construction scheme for the polarization propagator. *J Chem Theory Comput*. 2014;*10*:4583–98.

19. Rehn DR, Dreuw A, Norman P. Resonant inelastic X-ray scattering amplitudes and cross sections in the algebraic diagrammatic construction/intermediate state representation (ADC/ISR) approach. *J Chem Theory Comput*. 2017;*13*:5552–9.

20. Coriani S, Koch H. Communication: X-ray absorption spectra and core-ionization potentials within a core-valence separated coupled cluster framework. *J Chem Phys*. 2015;*143*:181103.

21. Peng B, Lestrange PJ, Goings JJ, Caricato M, Li X. Energy-specific equation- of-motion coupled-cluster methods for high-energy excited states: application to K-edge X-ray absorption spectroscopy. *J Chem Theory Comput*. 2015;*11*:4146–53.

22. Faber R, Coriani S. Resonant inelastic X-ray scattering and nonresonant X-ray emission spectra from coupled-cluster (damped) response theory. *J Chem Theory Comput*. 2019;*15*:520–8.

23. Vidal ML, Feng X, Epifanovsky E, Krylov AI, Coriani S. New and efficient equation-of-motion coupled-cluster framework for core-excited and core-ionized states. *J Chem Theory Comput*. 2019;*15*:3117–33.

24. Vidal ML, Krylov AI, Coriani S. Dyson orbitals within the fc-CVS-EOM-CCSD framework: theory and application to X-ray photoelectron spectroscopy of ground and excited states. *Phys Chem Chem Phys*. 2020;*22*:2693–703.

25. Vidal ML, Pokhilko P, Krylov AI, Coriani S. Equation-of-motion coupled-cluster theory to model L-edge X-ray absorption and photoelectron spectra. *J Phys Chem Lett*. 2020;*11*:8314–21.

26. Pinjari RV, Delcey MG, Guo M, Odelius M, Lundberg M. Restricted active space calculations of L-edge absorption spectra: from molecular orbitals to multiplet states. *J Chem Phys*. 2014;*141*:124116.

27. Allehyani BH, Hassan WI, Aziz SG, Hilal RH, Kühn O, Bokarev SI. Solvation and speciation of cobalt(II). A theoretical X-ray absorption and RIXS study. *Chem Phys*. 2020;*532*:110681.

28. Helmich-Paris B. Simulating X-ray absorption spectra with complete active space self-consistent field linear response methods. *Int J Quantum Chem*. 2021;*121*:e26559.

29. Koopmans T. Über Die Zuordnung von Wellenfunktionen Und Eigenwerten Zu Den Einzelnen Elektronen Eines Atoms. *Phys Ther*. 1934;*1*:104–13.

30. Bellafont NP, Bagus PS, Illas F. Prediction of core level binding energies in density functional theory: rigorous definition of initial and final state contributions and implications on the physical meaning of Kohn–Sham energies. *J Chem Phys*. 2015;*142*:214102.

31. Bagus PS, Schaefer HF. Direct near Hartree–Fock calculations on the 1s hole states of NO^+. *J Chem Phys*. 1971;*55*:1474–5.

32. Gilbert ATB, Besley NA, Gill PMW. Self-consistent field calculations of excited states using the maximum overlap method (MOM). *J Phys Chem A*. 2008;*112*:13164–71.

33. Besley NA, Gilbert ATB, Gill PMW. Self-consistent-field calculations of core excited states. *J Chem Phys*. 2009;*130*:124308.

34. Ye H-Z, Welborn M, Ricke ND, Van Voorhis T. σ-SCF: a direct energy-targeting method to mean-field excited states. *J Chem Phys*. 2017;*147*:214104.

35. Oosterbaan KJ, White AF, Head-Gordon M. Non-orthogonal configuration interaction with single substitutions for core-excited states: an extension to doublet radicals. *J Chem Theory Comput*. 2019;*15*:2966–73.

36. Hait D, Head-Gordon M. Excited state orbital optimization via minimizing the square of the gradient: general approach and application to singly and doubly excited states via density functional theory. *J Chem Theory Comput*. 2020;*16*:1699–710.

37. Levi G, Ivanov AV, Jónsson H. Variational density functional calculations of excited states via direct optimization. *J Chem Theory Comput*. 2020;*16*:6968–82.

38. Takahata Y, Chong DP. Estimation of Hammett sigma constants of substituted benzenes through accurate density-functional calculation of core–electron binding energy shifts. *Int J Quantum Chem*. 2005;*103*:509–15.

39. Kotsis K, Staemmler V. Ab initio calculations of the O1s XPS spectra of ZnO and Zn oxo compounds. *Phys Chem Chem Phys*. 2006;*8*:1490–8.

40. Takahata Y. Substituent effects in chain and ring π-systems studied by core–electron binding energies calculated by density functional theory. *Comput Theor Chem*. 2011;*978*:77–83.

41. Ershova OV, Besley NA. Theoretical calculations of the excited state potential energy surfaces of nitric oxide. *Chem Phys Lett*. 2012;*513*:179–83.

42. Trinh QT, Tan KF, Borgna A, Saeys M. Evaluating the structure of catalysts using core-level binding energies calculated from first principles. *J Phys Chem C*. 2013;*117*:1684–91.

43. Lüder J, de Simone M, Totani R, Coreno M, Grazioli C, Sanyal B, et al. The electronic characterization of biphenylene—experimental and theoretical insights from core and valence level spectroscopy. *J Chem Phys*. 2015;*142*:074305.

44. Santos AR, Hanson-Heine MWD, Besley NA, Licence P. The impact of sulfur functionalisation on nitrogen-based ionic liquid cations. *Chem Commun*. 2018;*54*:11403–6.

45. Pi JM, Stella M, Fernando NK, Lam AY, Regoutz A, Ratcliff LE. Predicting core level photoelectron spectra of amino acids using density functional theory. *J Phys Chem Lett*. 2020;*11*:2256–62.

46. Cavigliasso G, Chong DP. Accurate density-functional calculation of core–electron binding energies by a total-energy difference approach. *J Chem Phys*. 1999;*111*:9486–92.

47. Takahata Y, Chong DP. DFT calculation of core–electron binding energies. *J Electron Spectrosc Relat Phenom*. 2003;*133*:69–76.

48. Osamu Takahashi O, Pettersson LGM. Functional dependence of core-excitation energies. *J Chem Phys*. 2004;*121*:10339–45.

49. Segala M, Chong DP. K-shell core–electron binding energies for phosphorus- and sulfur-containing molecules calculated by density functional theory. *J Electron Spectrosc Relat Phenom*. 2010;*182*:141–4.

50. Tolbatov I, Chipman DM. Benchmarking density functionals and Gaussian basis sets for calculation of core–electron binding energies in amino acids. *Theor Chem Acc*. 2017;*136*:82.

51. Kahk JM, Lischner J. Accurate absolute core–electron binding energies of molecules, solids, and surfaces from first-principles calculations. *Phys Rev Mater*. 2019;*3*:10080.

52. Fouda AEA, Besley NA. Assessment of basis sets for density functional theory-based calculations of core–electron spectroscopies. *Theor Chem Acc*. 2018;*137*:6.

53. Krylov AI. Equation-of-motion coupled-cluster methods for open-shell and electronically excited species: the Hitchhiker's guide to Fock space. *Annu Rev Phys Chem*. 2008;*59*:433–62.

54. Stephens PJ, Devlin FJ, Chabolowski CH, Frisch MJ. Ab initio calculation of vibrational absorption and circular dichroism spectra using density functional force fields. *J Phys Chem*. 1994;*98*:11623–7.

55. Yanai T, Tew DP, Handy NC. A new hybrid exchange–correlation functional using the Coulomb-attenuating method (CAM-B3LYP). *Chem Phys Lett*. 2004;*393*:51–7.

56. Karton A, Tarnopolsky A, Lamere JF, Schatz GC, Martin JML. Highly accurate first-principles benchmark data sets for the parametrization and validation of density functional and other approximate methods. Derivation of a robust, generally applicable, double-hybrid functional for thermochemistry and thermochemical kinetics. *J Phys Chem A*. 2008;*112*:12868–86.

57. Hanson-Heine MWD, George MW, Besley NA. Basis sets for the calculation of core–electron binding energies. *Chem Phys Lett*. 2018;*699*:279–85.

58. Sarangi R, Vidal ML, Coriani S, Krylov AI. On the basis set selection for calculations of core-level states: different strategies to balance cost and accuracy. *Mol Phys*. 2020;*118*:e1769872.

59. Ambroise MA, Jensen F. Probing basis set requirements for calculating core ionization and core excitation spectroscopy by the Δself-consistent-field approach. *J Chem Theory Comput*. 2019;*8*:325–37.

60. Carniato S, Milliè P. Accurate core electron binding energy calculations using small 6−31G and TZV core hole optimized basis sets. *J Chem Phys*. 2002;*116*:3521–32.

61. Schindler M, Kutzelnigg W. Theory of magnetic susceptibilities and NMR chemical shifts in terms of localized quantities. II. Application to some simple molecules. *J Chem Phys*. 1982;*76*:1919–33.

62. Mijovilovich A, Pettersson LGM, Mangold S, Janousch M, Susini J, Salome M, et al. The interpretation of sulfur K-edge XANES spectra: a case study on thiophenic and aliphatic sulfur compounds. *J Phys Chem A*. 2009;*113*:2750–6.

63. Fransson T, Zhovtobriukh I, Coriani S, Wikfeldt KT, Norman P, Pettersson LGM. Requirements of first-principles calculations of X-ray absorption spectra of liquid water. *Phys Chem Chem Phys*. 2016;*18*:566–83.

64. Zhovtobriukh I, Besley NA, Fransson T, Nilsson A, Pettersson LGM. Relationship between X-ray emission and absorption spectroscopy and the local H-bond environment in water. *J Chem Phys*. 2018;*148*:144507.

65. Mårtensson N, Nilsson A. On the origin of core-level binding energy shifts. *J Electron Spectrosc Relat Phenom*. 1995;*75*:209–23.

66. Plashkevych O, Privalov T, Ågren H, Carravetta V, Ruud K. On the validity of the equivalent cores approximation for computing X-ray photoemission and photoabsorption spectral bands. *Chem Phys*. 2000;*260*:11–28.

67. Delesma FA, Van den Bossche M, Grönbeck H, Calaminici P, Köster AM, LGM P. A chemical view on X-ray photoelectron spectroscopy: the ESCA molecule and surface-to-bulk XPS shifts. *ChemPhysChem*. 2018;*19*:169–74.

68. Diesen E, Rodrigues GLS, Luntz AC, Abild-Pedersen F, Pettersson LGM, Voss J. Accuracy of XAS theory for unraveling structural changes of adsorbates: CO on Ni(100). *AIP Adv*. 2020;*10*:115014.

69. Hedin L. New method for calculating the one-particle Green's function with application to the electron-gas problem. *Phys Rev*. 1965; *139*:A796–822.

70. Aryasetiawan F, Gunnarsson O. The *GW* method. *Rep Prog Phys*. 1998;*61*:237–312.

71. van Setten MJ, Costa R, Viñes F, Illas F. Assessing *GW* approaches for predicting core level binding energies. *J Chem Theory Comput*. 2018;*14*:877–883.

72. Golze D, Keller L, Rinke P. Accurate absolute and relative core-level binding energies from *GW*. *J Phys Chem Lett*. 2020;*11*:1840–7.

73. Ortiz JV. Dyson-orbital concepts for description of electrons in molecules. *J Chem Phys*. 2020;*153*:070902.

74. Green JC, Decleva P. Photoionization cross-sections: a guide to electronic structure. *Coord Chem Rev*. 2005;*249*:209–28.

75. Gelius U, Siegbahn K. ESCA studies of molecular core and valence levels in the gas phase. *Faraday Discuss Chem Soc*. 1972;*54*:257–68.

76. Nilsson A, Pettersson LGM. Chemical bonding on surfaces probed by X-ray emission spectroscopy and density functional theory. *Surf Sci Rep*. 2004;*55*:49–167.

77. Wernet P, Nordlund D, Bergmann U, Cavalleri M, Odelius M, Ogasawara H, et al. The structure of the first coordination shell of liquid water. *Science*. 2004;*304*:995–9.

78. Wilson KR, Cavalleri M, Rude BS, Schaller RD, Catalano T, Nilsson A, et al. X-ray absorption spectroscopy of liquid methanol microjets: bulk electronic structure and hydrogen bonding network. *J Phys Chem B*. 2005;*109*:10194–203.

79. Fransson T, Harada Y, Kosugi N, Besley NA, Winter B, Pettersson LGM, et al. X-ray and electron spectroscopy of water. *Chem Rev*. 2016;*116*:7551–69.

80. Solomon EI, Szilagyi RK, George SD, Basumallick L. Electronic structures of metal sites in proteins and models: contributions to function in blue copper proteins. *Chem Rev*. 2004;*104*:419–58.

81. Dell'Angela M, Anniyev T, Beye M, Coffee R, Föhlisch A, Gladh J, et al. Real-time observation of surface bond breaking with an X-ray laser. *Science*. 2013;*339*:1302–5.

82. Derricotte WD, Evangelista FA. Simulation of X-ray absorption spectra with orthogonality constrained density functional theory. *Phys Chem Chem Phys*. 2015;*17*:14360–74.

83. Ågren H, Carravetta V, Vahtras O, Pettersson LGM. Direct, atomic orbital, static exchange calculations of photoabsorption spectra of large molecules and clusters. *Chem Phys Lett*. 1994;*222*:75–81.

84. Stener M, Lisini A, Decleva P. Density functional calculations of excitation energies and oscillator strengths for C1s → π* and O1s → π* excitations and ionization potentials in carbonyl containing molecules. *Chem Phys*. 1995;*191*:141–54.

85. Triguero L, Pettersson LGM, Ågren H. Calculations of near-edge X-ray-absorption spectra of gas-phase and chemisorbed molecules by means of density-functional and transition-potential theory. *Phys Rev B*. 1998;*58*:8097–110.

86. Oosterbaan KJ, White AF, Head-Gordon M. Non-orthogonal configuration interaction with single substitutions for the calculation of core-excited states. *J Chem Phys*. 2018;*149*:044116.

87. Oosterbaan KJ, White AF, Hait D, Head-Gordon M. Generalized single excitation configuration interaction: an investigation into the impact of the inclusion of non-orthogonality on the calculation of core-excited states. *Phys Chem Chem Phys*. 2020;*22*: 8182–92.

88. Prendergast D, Galli G. X-ray absorption spectra of water from first principles calculations. *Phys Rev Lett*. 2006;*96*:215502.

89. Su GM, Patel SN, Pemmaraju CD, Prendergast D, Chabinyc ML. First-principles predictions of near-edge X-ray absorption fine structure spectra of semiconducting polymers. *J Phys Chem C*. 2017;*121*:9142–52.

90. Poloni R, Mariano AL, Prendergast D, Garcia-Barriocanal J. Probing the electric field-induced doping mechanism in $YBa_2Cu_3O_7$ using computed Cu K-edge X-ray absorption spectra. *J Chem Phys*. 2018;*149*:234706.

91. Rundel K, Liang Y, Welford A, Prendergast D, McNeill CR. Understanding the effect of thionation on naphthalene diimide using first-principles predictions of near-edge X-ray absorption fine structure spectra. *J Chem Phys*. 2019;*150*:104302.

92. Soininen JA, Shirley EL. Scheme to calculate core hole–electron interactions in solids. *Phys Rev B*. 2001;*64*:165112.

93. Shirley EL. Bethe–Salpeter treatment of X-ray absorption including core-hole multiplet effects. *J Electron Spectrosc Relat Phenom*. 2005; *144–147*:1187–90.

94. Rehr JJ, Soininen JA, Shirley EL. Final-state rule vs the Bethe–Salpeter equation for deep-core X-ray absorption spectra. *Phys Scr*. 2005; *T115*:207–11.

95. Gilmore K, Vinson J, Shirley EL, Prendergast D, Pemmaraju CD, Kas JJ, et al. Efficient implementation of core-excitation Bethe–Salpeter equation calculations. *Comput Phys Commun*. 2015;*197*:109–17.

96. Olovsson W, Tanaka I, Mizoguchi T, Puschnig P, Ambrosch-Draxl C. All-electron Bethe–Salpeter calculations for shallow-core X-ray absorption near-edge structures. *Phys Rev B*. 2009;*79*:041102.

97. Vinson J, Rehr JJ. Ab initio Bethe–Salpeter calculations of the X-ray absorption spectra of transition metals at the L-shell edges. *Phys Rev B*. 2012;*86*:195135.

98. Leng X, Jin F, Wei M, Ma Y. *GW* method and Bethe–Salpeter equation for calculating electronic excitations. *WIREs Comput Mol Sci*. 2016;*6*:532–50.

99. Onida G, Reining L, Rubio A. Electronic excitations: density-functional versus many-body Green's-function approaches. *Rev Mod Phys*. 2002;*74*:601–59.

100. Fronzoni G, Stener M, Decleva P. Theoretical study of the excited and continuum states in the NEXAFS regions of Cl_2. *Phys Chem Chem Phys*. 1999;*1*:1405–14.

101. Fronzoni G, Stener M, Decleva P. Valence and core photoionization dynamics of acetylene by TD-DFT continuum approach. *Chem Phys*. 2004;*298*:141–53.

102. Hirata S, Head-Gordon M. Time-dependent density functional theory within the Tamm–Dancoff approximation. *Chem Phys Lett*. 1999;*314*:291–9.

103. Stener M, Fronzoni G, de Simone M. Time dependent density functional theory of core electrons excitations. *Chem Phys Lett*. 2003;*373*:115–23.

104. Cederbaum LS, Domcke W, Schirmer J. Many-body theory of core holes. *Phys Rev A*. 1980;*22*:206–22.

105. Tsuchimochi T, Kobayashi M, Nakata A, Imamura Y, Nakai H. Application of the Sakurai-Sugiura projection method to core-excited-state calculation by time-dependent density functional theory. *J Comput Chem*. 2008;*29*:2311–6.

106. Ekström U, Norman P. X-ray absorption spectra from the resonant-convergent first-order polarization propagator approach. *Phys Rev A*. 2006;*74*:042722.

107. Ekström U, Norman P, Carravetta V, Ågren H. Polarization propagator for X-ray spectra. *Phys Rev Lett*. 2006;*97*:143001.

108. Robinson D, Besley NA. Modelling the spectroscopy and dynamics of plastocyanin. *Phys Chem Chem Phys*. 2010;*12*:9667–76.

109. Schmidt N, Fink R, Hieringer W. Assignment of near-edge X-ray absorption fine structure spectra of metalloporphyrins by means of time-dependent density-functional calculations. *J Chem Phys*. 2010;*133*:054703.

110. Buckley MW, Besley NA. A theoretical study of the near-edge X-ray absorption fine structure of amino acids and proteins. *Chem Phys Lett*. 2011;*501*:540–6.

111. Lima FA, Bjornsson R, Weyhermüller T, Chandrasekaran P, Glatzel P, Neese F, et al. High-resolution molybdenum K-edge X-ray absorption spectroscopy analyzed with time-dependent density functional theory. *Phys Chem Chem Phys*. 2013;*15*:20911–20.

112. Ljubic I, Kivimaki A, Coreno M. An experimental NEXAFS and computational TDDFT and DeltaDFT study of the gas-phase core excitation spectra of nitroxide free radical TEMPO and its analogues. *Phys Chem Chem Phys*. 2016;*18*:10207–17.

113. De Francesco R, Stener M, Fronzoni G. TDDFT calculations of NEXAFS spectra of model systems for SO_2 adsorbed on the MgO(100) surface. *J Phys Chem C*. 2007;*111*:13554–63.

114. Besley NA, Noble A. Time-dependent density functional theory study of the X-ray absorption spectroscopy of acetylene, ethylene, and benzene on Si(100). *J Phys Chem C*. 2007;*111*:3333–40.

115. Fogarty RM, Matthews RP, Clough MT, Ashworth CR, Brandt A, Corbett PJ, et al. NEXAFS spectroscopy of ionic liquids: experiments versus calculations. *Phys Chem Chem Phys*. 2017;*19*:31156–67.

116. Löble MW, Keith JM, Altman AB, Stieber SCE, Batista ER, Boland KS, et al. Covalency in lanthanides. An X-ray absorption spectroscopy and density functional theory study of $LnCl_6^{x-}$ ($x = 3$, 2). *J Am Chem Soc*. 2015;*137*:2506–23.

117. Liao M-S, Watts JD, Huang M-J. DFT/TDDFT study of lanthanide(III) mono- and bisporphyrin complexes. *J Phys Chem A*. 2006;*110*:13089–98.

118. Forbes R, Pratt ST, De Fanis A, Milosavljevic AR, Nicolas C, Bozek JD, et al. Photoabsorption, photoionization, and Auger processes at the carbon K-edge in CH_3I. *Phys Rev A*. 2020;*101*:023408.

119. Hsu H, Davidson ER, Pitzer RM. SCF method for hole states. *J Chem Phys*. 1976;*65*:609–13.

120. Leininger ML, Sherrill CD, Allen WD, Schaefer HF III. Systematic study of selected diagonalization methods for configuration interaction matrices. *J Comput Chem*. 2001;*22*:1574–89.

121. Li X, Govind N, Isborn C, Eugene DePrince A III, Lopata K. Real-time time-dependent electronic structure theory. *Chem Rev*. 2020;*120*:9951–93.

122. Lopata K, Van Kuiken BE, Khalil M, Govind N. Linear-response and real-time time-dependent density functional theory studies of core-level near-edge X-ray absorption. *Chem Theory Comput*. 2012;*8*:3284–92.

123. Skowron ST, Besley NA. Time-dependent density functional theory calculations of the near edge X-ray absorption fine structure of large systems. *Theor Chem Acc*. 2012;*131*:1267.

124. Besley NA. Fast time-dependent density functional theory calculations of the X-ray absorption spectroscopy of large systems. *J Chem Theory Comput*. 2016;*12*:5018–25.

125. Hanson-Heine MWD, George MW, Besley NA. Assessment of time-dependent density functional theory with the restricted excitation space approximation for excited state calculations of large systems. *Mol Phys*. 2018;*116*:1452–9.

126. Maganas D, DeBeer S, Neese F. A restricted open configuration interaction with singles method to calculate valence-to-core resonant X-ray emission spectra: a case study. *Inorg Chem*. 2017;*56*:11819–36.

127. da Cruz VV, Eckert S, Föhlisch A. TD-DFT simulations of K-edge resonant inelastic X-ray scattering within the restricted subspace approximation. *Phys Chem Chem Phys*. 2021;*23*:1835–48.

128. Besley NA, Peach MJG, Tozer DJ. Time-dependent density functional theory calculations of near-edge X-ray absorption fine structure with short-range corrected functionals. *Phys Chem Chem Phys*. 2009;*11*:10350–8.

129. Kasper JM, Stetina TF, Jenkins AJ, Li X. Ab initio methods for L-edge X-ray absorption spectroscopy. *Chem Phys Rev*. 2020;*1*:011304.

130. Fronzoni G, Stener M, Decleva P, Wang F, Ziegler T, Van Lenthe E, et al. Spin–orbit relativistic time dependent density functional theory calculations for the description of core electron excitations: TiCl$_4$ case study. *Chem Phys Lett*. 2005;*416*:56–63.

131. Fronzoni G, Stener M, Decleva P, de Simone M, Coreno M, Franceschi P, et al. X-ray absorption spectroscopy of VOCl$_3$, CrO$_2$Cl$_2$, and MnO$_3$Cl: an experimental and theoretical study. *J Phys Chem A*. 2009;*113*:2914–25.

132. Josefsson I, Kunnus K, Schreck S, Föhlisch A, de Groot F, Wernet P, et al. Ab initio calculations of X-ray spectra: atomic multiplet and molecular orbital effects in a multiconfigurational SCF approach to the L-edge spectra of transition metal complexes. *J Phys Chem Lett*. 2012;*3*:3565–70.

133. Pinjari RV, Delcey MG, Guo M, Odelius M, Lundberg M. Restricted active space calculations of L-edge X-ray absorption spectra: from molecular orbitals to multiplet states. *J Chem Phys*. 2014;*141*:124116.

134. Roemelt M, Neese F. Excited states of large open-shell molecules: an efficient, general, and spin-adapted approach based on a restricted open-shell ground state wave function. *J Phys Chem A*. 2013;*117*:3069–83.

135. Roemelt M, Maganas D, DeBeer S, Neese F. A combined DFT and restricted open-shell configuration interaction method including spin-orbit coupling: application to transition metal L-edge X-ray absorption spectroscopy. *J Chem Phys*. 2013;*138*:204101.

136. Stetina TF, Kasper JM, Li X. Modeling L$_{2,3}$-edge X-ray absorption spectroscopy with linear response exact two-component relativistic time-dependent density functional theory. *J Chem Phys*. 2019;*150*:234103.

137. Kadek M, Konecny L, Gao B, Repisky M, Ruud K. X-ray absorption resonances near L$_{2,3}$-edges from real-time propagation of the Dirac–Kohn–Sham density matrix. *Phys Chem Chem Phys*. 2015;*17*:22566–70.

138. Fransson T, Burdakova D, Norman P. K- and L-edge X-ray absorption spectrum calculations of closed-shell carbon, silicon, germanium, and sulfur compounds using damped four-component density functional response theory. *Phys Chem Chem Phys*. 2016;*18*: 13591–603.

139. Nakata A, Imamura Y, Nakai H. Hybrid exchange–correlation functional for core, valence, and Rydberg excitations: core-valence-Rydberg B3LYP. *J Chem Phys*. 2006;*125*:064109.

140. Nakata A, Imamura Y, Nakai H. Extension of the core-valence-Rydberg B3LYP functional to core-excited-state calculations of third-row atoms. *J Chem Theory Comput*. 2007;*3*:1295–305.

141. Imamura Y, Nakai H. Analysis of self-interaction correction for describing core excited states. *Int J Quantum Chem*. 2007;*107*:23–9.

142. Tu G, Rinkevicius Z, Vahtras O, Ågren H, Ekström U, Norman P, et al. Self-interaction-corrected time-dependent density-functional-theory calculations of X-ray-absorption spectra. *Phys Rev A*. 2007;*76*:022506.

143. DeBeer George S, Petrenko T, Neese F. Prediction of iron K-edge absorption spectra using time-dependent density functional theory. *J Phys Chem A*. 2008;*112*:12936–43.

144. DeBeer George S, Petrenko T, Neese F. Time-dependent density functional calculations of ligand K-edge X-ray absorption spectra. *Inorg Chem Acta*. 2008;*361*:965–972.

145. Lestrange PJ, Nguyen PD, Li X. Calibration of energy-specific TDDFT for modeling K-edge XAS spectra of light element. *J Chem Theory Comput*. 2015;*11*:2994–9.

146. Fransson T, Brumboiu MI, Vidal ML, Norman P, Coriani S, Dreuw A. XABOOM: an X-ray absorption benchmark of organic molecules based on carbon, nitrogen, and oxygen 1s→π* transitions. *J Chem Theory Comput*. 2021; in press. https://10.1021/acs.jctc.0c01082.

147. Song J-W, Watson MA, Nakata A, Hirao K. Core-excitation energy calculations with a long-range corrected hybrid exchange–correlation functional including a short-range Gaussian attenuation (LCgau-BOP). *J Chem Phys*. 2008;*129*:184113.

148. Capano G, Penfold TJ, Besley NA, Milne CJ, Reinhard M, Rittmann-Frank H, et al. The role of Hartree–Fock exchange in the simulation of X-ray absorption spectra: a study of photoexcited [Fe(bpy)$_3$]$^{2+}$. *Chem Phys Lett*. 2013;*580*:179–84.

149. Jin Y, Bartlett RJ. The QTP family of consistent functionals and potentials in Kohn–Sham density functional theory. *J Chem Phys*. 2016;*145*:034107.

150. Jin Y, Bartlett RJ. Accurate computation of X-ray absorption spectra with ionization potential optimized global hybrid functional. *J Chem Phys*. 2018;*149*:064111.

151. Bressler C, Milne C, Pham V-T, El Nahhas A, van der Veen RM, Gawelda W, et al. Femtosecond XANES study of the light-induced spin crossover dynamics in an iron(II) complex. *Science*. 2009;*323*:489–92.

152. Bartlett SA, Besley NA, Dent AJ, Evans J, Hamilton ML, Hanson-Heine MWD, et al. Monitoring the formation and reactivity of organometallic alkane and fluoroalkane complexes with silanes and Xe using time-resolved XAFS. *J Am Chem Soc*. 2019;*141*: 11471–80.

153. Wolf TJA, Myhre RH, Cryan JP, Coriani S, Squibb RJ, Battistoni A, et al. Probing ultrafast ππ*/nπ* internal conversion in organic chromophores via K-edge resonant absorption. *Nat Commun*. 2017;*8*:29.

154. Chang KF, Reduzzi M, Wang H, Poullain SM, Kobayashi Y, Barreau L, et al. Revealing electronic state-switching at conical intersections in alkyl iodides by ultrafast XUV transient absorption spectroscopy. *Nat Commun*. 2020;*11*:4042.

155. Capano G, Milne CJ, Chergui M, Rothlisberger U, Tavernelli I, Penfold TJ. Probing wavepacket dynamics using ultrafast X-ray spectroscopy. *J Phys B: At Mol Opt Phys*. 2015;*48*:214001.

156. Penfold TJ, Pápai M, Rozgonyi T, Møller KB, Vankó G. Probing spin–vibronic dynamics using femtosecond X-ray spectroscopy. *Faraday Discuss*. 2016;*194*:731–46.

157. Bhattacherjee A, Leone SR. Ultrafast X-ray transient absorption spectroscopy of gas-phase photochemical reactions: a new universal probe of photoinduced molecular dynamics. *Acc Chem Res*. 2018;*51*:3203–11.

158. Attar AR, Bhattacherjee A, Pemmaraju CD, Schnorr K, Closser KD, Prendergast D, et al. Femtosecond X-ray spectroscopy of an electrocyclic ring-opening reaction. *Science*. 2017;*356*:54–9.

159. Heller EJ. Time-dependent approach to semiclassical dynamics. *J Chem Phys*. 1975;*62*:1544–55.

160. Heller EJ. Frozen Gaussians: a very simple semiclassical approximation. *J Chem Phys*. 1981;*75*:2923–31.

161. Worth GA, Burghardt I. Full quantum mechanical molecular dynamics using Gaussian wavepackets. *Chem Phys Lett*. 2003;*368*:502–8.

162. Richings GW, Worth GA. A practical diabatisation scheme for use with the direct-dynamics variational multi-configuration Gaussian method. *J Phys Chem A*. 2015;*119*:12457–70.

163. Northey T, Duffield J, Penfold TJ. Non-equilibrium X-ray spectroscopy using direct quantum dynamics. *J Chem Phys*. 2018;*149*:124107.

164. Northey T, Norell J, Fouda AEA, Besley NA, Odelius M, Penfold TJ. Ultrafast nonadiabatic dynamics probed by nitrogen K-edge absorption spectroscopy. *Phys Chem Chem Phys*. 2020;*22*:2667–76.

165. Lee N, Petrenko T, Bergmann U, Neese F, DeBeer S. Probing valence orbital composition with iron Kβ X-ray emission epectroscopy. *J Am Chem Soc*. 2010;*132*:9715–27.

166. Hanson-Heine MWD, George MW, Besley NA. Kohn–Sham density functional theory calculations of non-resonant and resonant X-ray emission spectroscopy. *J Chem Phys*. 2017;*146*:094106.

167. Hanson-Heine MWD, George MW, Besley NA. Density functional theory calculations of the non-resonant and resonant X-ray emission spectroscopy of carbon fullerenes and nanotubes. *Chem Phys Lett*. 2018;*696*:119–24.

168. Wadey JD, Besley NA. Quantum chemical calculations of X-ray emission spectroscopy. *J Chem Theory Comput*. 2014;*10*:4557–64.

169. Besley NA. Equation of motion coupled cluster theory calculations of the X-ray emission spectroscopy of water. *Chem Phys Lett*. 2012;*542*:42–6.

170. Fransson T, Dreuw A. Simulating X-ray emission spectroscopy with algebraic diagrammatic construction schemes for the polarization propagator. *J Chem Theory Comput*. 2019;*15*:546–56.

171. Fouda AEA, Besley NA. Improving the predictive quality of time-dependent density functional theory calculations of the X-ray emission spectroscopy of organic molecules. *J Comput Chem*. 2020;*41*:1081–90.

172. Foerster A, Besley NA. Time-dependent density functional theory study of the X-ray emission spectroscopy of amino acids and proteins. *Chem Phys Lett*. 2020;*757*:137860.

173. Zhang Y, Mukamel S, Khalil M, Govind N. Simulating valence-to-core X-ray emission spectroscopy of transition metal complexes with time-dependent density functional theory. *J Chem Theory Comput*. 2015;*11*:5804–9.

174. Roper IPE, Besley NA. The effect of basis set and exchange–correlation functional on time-dependent density functional theory calculations within the Tamm–Dancoff approximation of the X-ray emission spectroscopy of transition metal complexes. *J Chem Phys*. 2016;*144*:114104.

175. Mortensen DR, Seidler GT, Kas JJ, Govind N, Schwartz CP, Pemmaraju S, et al. Benchmark results and theoretical treatments for valence-to-core X-ray emission spectroscopy in transition metal compounds. *Phys Rev B*. 2017;*96*:125136.

176. Clarke CJ, Hayama S, Hawes A, Hallett JP, Chamberlain TW, Lovelock KRJ, et al. Zinc 1s valence-to-core X-ray emission spectroscopy of halozincate complexes. *J Phys Chem A*. 2019;*123*:9552–9.

177. Jahrman EP, Rana J, Fister TT, Holden WM, Govind N, Kas JJ, et al. Valence-to-core X-ray emission spectroscopy of vanadium oxide and lithiated vanadyl phosphate materials. *J Mater Chem A*. 2020;*8*:16332–44.

178. Rehr JJ, Kas JJ, Vila FD, Prange MP, Jorissen K. Parameter-free calculations of X-ray spectra with FEFF9. *Phys Chem Chem Phys*. 2010;*12*:5503–13.

179. Rehr JJ. Theory and calculations of X-ray spectra: XAS, XES, XRS, and NRIXS. *Radiat Phys Chem*. 2006;*75*:1547–58.

180. Rubensson J-E, Wassdahl N, Brammer R, Nordgren J. Local electronic structure in simple alcohols studied in X-ray emission. *J Electron Spectrosc Relat Phenom*. 1988;*47*:131–45.

181. Nordgren J, Ågren H, Werme LO, Nordling C, Siegbahn K. X-ray emission spectra of NH_3 and N_2O. *J Phys B: At Mol Phys*. 1976;*9*:295–302.

182. Lindle DW, Cowan PL, Jach T, LaVilla RE, Deslattes RD, Perera RCC. Polarized X-ray emission studies of methyl chloride and the chlorofluoromethanes. *Phys Rev A*. 1991;*43*:2353–66.

183. MacMillan SN, Walroth RC, Perry DM, Morsing TJ, Lancaster KM. Ligand-sensitive but not ligand-diagnostic: evaluating Cr valence-to-core X-ray emission spectroscopy as a probe of inner-sphere coordination. *Inorg Chem*. 2015;*54*:205–14.

184. Pollock CJ, DeBeer S. Valence-to-core X-ray emission spectroscopy: a sensitive probe of the nature of a bound ligand. *J Am Chem Soc*. 2011;*133*:5594–601.

185. Atkins AJ, Bauer M, Jacob CR. The chemical sensitivity of X-ray spectroscopy: high energy resolution XANES versus X-ray emission spectroscopy of substituted ferrocenes. *Phys Chem Chem Phys*. 2013;*15*:8095–105.

186. Oung SW, Rudolph J, Jacob CR. Uncertainty quantification in theoretical spectroscopy: the structural sensitivity of X-ray emission spectra. *Int J Quantum Chem*. 2018;*118*:e25458.

187. Smolentsev G, Soldatov AV, Messinger J, Merz K, Weyhermueller T, Bergmann U, et al. X-ray emission spectroscopy to study ligand valence orbitals in Mn coordination complexes. *J Am Chem Soc*. 2009;*131*:13161–7.

188. Beckwith MA, Roemelt M, Collomb MN, DuBoc C, Weng T-C, Bergmann U, et al. Manganese Kβ X-ray emission spectroscopy as a probe of metal–ligand interactions. *Inorg Chem*. 2011;*50*:8397–409.

189. Delgado-Jaime MU, Dible BR, Chiang KP, Brennessel WW, Bergmann U, Holland PL, et al. Identification of a single light atom within a multinuclear metal cluster using valence-to-core X-ray emission spectroscopy. *Inorg Chem*. 2011;*50*:10709–17.

190. Pollock CJ, DeBeer S. Insights into the geometric and electronic structure of transition metal centers from valence-to-core X-ray emission spectroscopy. *Acc Chem Res*. 2015;*48*:2967–75.

191. Rees JA, Wandzilak A, Maganas D, Wurster NIC, Hugenbruch S, Kowalska JK, et al. Experimental and theoretical correlations between vanadium K-edge X-ray absorption and Kβ emission spectra. *J Biol Inorg Chem*. 2016;*21*:793–805.

192. Burkhardt L, Vukadinovic Y, Nowakowski M, Kalinko A, Rudolph J, Carlsson P-A, et al. Electronic structure of the Hieber anion [Fe(CO)$_3$(NO)]$^-$ revisited by X-ray emission and absorption spectroscopy. *Inorg Chem*. 2020;*59*:3551–61.

193. Bernadotte S, Atkins AJ, Jacob CR. Origin-independent calculation of quadrupole intensities in X-ray spectroscopy. *J Chem Phys*. 2012;*137*:204106.

194. Otsuka T, Chong DP, Maki J, Kawabe H, Endo K. Theoretical Auger electron and X-ray emission spectra of CO and H_2O by density functional theory calculations. *Chem Phys Lett*. 2002;*352*:511–20.

195. Puska MJ, Nieminen RM. Density-functional calculations of Auger and X-ray photoemission shifts for metallic elements. *Phys Scr*. 1982;*25*:708–12.

196. Forbes R, De Fanis A, Bomme C, Rolles S, Pratt ST, Powis I, et al. Auger electron angular distributions following excitation or ionization of the I 3d level in methyl iodide. *J Chem Phys*. 2018;*149*:094304.

197. Zhu H, Yang Y, Hyeon-Deuk K, Califano M, Song N, Wang Y, et al. Auger-assisted electron transfer from photoexcited semiconductor quantum dots. *Nano Lett*. 2014;*14*:1263–9.

198. Zhou G, Lu G, Prezhdo OV. Modeling Auger processes with nonadiabatic molecular dynamics. *Nano Lett*. 2021;*21*:756–61.

199. Penent F, Nakano M, Tashiro M, Grozdanov TP, Žitnik M, Bučar K, et al. Double core hole spectroscopy with synchrotron radiation. *J Electron Spectrosc Relat Phenom*. 2015;*204*:303–12.

200. Lablanquie P, Penent F, Hikosaka Y. Multi-electron coincidence spectroscopy: double photoionization from molecular inner-shell orbitals. *J Phys B: At Mol Opt Phys*. 2016;*49*:182002.

201. Nakano M, Penent F, Tashiro M, Grozdanov TP, Žitnik M, Carniato S, et al. Single photon K^{-2} and $K^{-1}K^{-1}$ double core ionization in C_2H_{2n} ($n = 1$–3), CO, and N_2 as a potential new tool for chemical analysis. *Phys Rev Lett*. 2013;*110*:163001.

202. Carniato S, Selles P, Andric L, Palaudoux J, Penent F, Žitnik M, et al. Single photon simultaneous K-shell ionization and K-shell excitation. I. Theoretical model applied to the interpretation of experimental results on H_2O. *J Chem Phys*. 2015;*142*:014307.

203. Zheng X, Liu J, Doumy G, Young L, Cheng L. Hetero-site double core ionization energies with sub-electronvolt accuracy from delta-coupled-cluster calculations. *J Phys Chem A*. 2020;*124*:4413–26.

204. Ament LJP, van Veenendaal M, Devereaux TP, Hill JP, van den Brink J. Resonant inelastic X-ray scattering studies of elementary excitations. *Rev Mod Phys*. 2011;*83*:705–767.

205. Weinhardt L, Benkert A, Meyer F, Blum M, Wilks RG, Yang W, et al. Nuclear dynamics and spectator effects in resonant inelastic soft X-ray scattering of gas-phase water molecules. *J Chem Phys*. 2012;*136*:144311.

206. Blum M, Odelius M, Weinhardt L, Pookpanratana S, Bär M, Zhang Y, et al. Ultrafast proton dynamics in aqueous amino acid solutions studied by resonant inelastic soft X-ray scattering. *J Phys Chem B*. 2012;*116*:13757–64.

207. Weinhardt L, Ertan E, Iannuzzi M, Weigand M, Fuchs O, Baer M, et al. Probing hydrogen bonding orbitals: resonant inelastic soft X-ray scattering of aqueous NH_3. *Phys Chem Chem Phys*. 2015;*17*:27145–53.

208. Benkert A, Meyer F, Hauschild D, Blum M, Yang W, Wilks RG, et al. Isotope effects in the resonant inelastic soft X-ray scattering maps of gas-phase methanol. *J Phys Chem A*. 2016;*120*:2260–2267.

209. Guo J, Luo Y. Molecular structure in water and solutions studied by photon-in/photon-out soft X-ray spectroscopy. *J Electron Spectrosc Relat Phenom*. 2010;*177*:181–91.

210. Weinhardt L, Fuchs O, Blum M, Bär M, Weigand M, Denlinger J, et al. Resonant X-ray emission spectroscopy of liquid water: novel instrumentation, high resolution, and the map approach. *J Electron Spectrosc Relat Phenom*. 2010;*177*:206–211.

211. Faber R, Coriani S. Core–valence-separated coupled-cluster-singles-and-doubles complex-polarization-propagator approach to X-ray spectroscopies. *Phys Chem Chem Phys*. 2020;*22*:2642–7.

212. Nanda KD, Vidal ML, Faber R, Coriani S, Krylov AI. How to stay out of trouble in RIXS calculations within equation-of-motion coupled-cluster damped response theory? Safe hitchhiking in the excitation manifold by means of core–valence separation. *Phys Chem Chem Phys*. 2020;*22*:2629–41.

213. Kjellsson L, Nanda KD, Rubensson J-E, Doumy G, Southworth SH, Ho PJ, et al. Resonant inelastic X-ray scattering reveals hidden local transitions of the aqueous OH radical. *Phys Rev Lett*. 2020;*124*:236001.

214. Fouda AEA, Purnell GI, Besley NA. Simulation of ultra-fast dynamics effects in resonant inelastic X-ray scattering of gas-phase water. *J Chem Theory Comput*. 2018;*14*:2586–95.

215. Kramers HA, Heisenberg W. Über die streuung von strahlung durch atome. *Z Phys*. 1925;*31*:681–708.

216. Gel'mukhanov F, Ågren H. Resonant inelastic X-ray scattering with symmetry-selective excitation. *Phys Rev A: At Mol Opt Phys*. 1994;*49*:4378–89.

217. Luo Y, Ågren H, Gel'mukhanov F. Symmetry assignments of occupied and unoccupied molecular orbitals through spectra of polarized resonance inelastic X-ray scattering. *J Phys B: At Mol Opt Phys*. 1994;*27*:4169–80.

218. Luo Y, Ågren H, Gel'mukhanov F. Polarization anisotropy in resonant X-ray emission from molecules. *Phys Rev A: At Mol Opt Phys*. 1996;*53*:1340–8.

219. Gel'mukhanov F, Ågren H. Resonant X-ray Raman scattering. *Phys Rep*. 1999;*312*:87–330.

220. Ljungberg MP, Nilsson A, Pettersson LGM. Semiclassical description of nuclear dynamics in X-ray emission of water. *Phys Rev B: Condens Matter Mater Phys*. 2010;*82*:245115.

221. Ljungberg M, Zhovtobriukh I, Takahashi O, Pettersson LGM. Core-hole-induced dynamical effects in the X-ray emission spectrum of liquid methanol. *J Chem Phys*. 2017;*146*:134506.

222. Takahashi O, Ljungberg MP, Pettersson LGM. X-ray emission spectrum of liquid ethanol: origin of split peaks. *J Phys Chem B*. 2017;*121*:11163–8.

223. Ljungberg MP. Vibrational effects in X-ray absorption and resonant inelastic X-ray scattering using a semiclassical scheme. *Phys Rev B: Condens Matter Mater Phys*. 2017;*96*:214302.

224. Fouda AEA, Seitz LC, Hauschild D, Blum M, Yang W, Heske C, et al. Observation of double excitations in the resonant inelastic X-ray scattering of nitric oxide. *J Phys Chem Lett*. 2020;*11*:7476–82.